Publication Year	2019
Acceptance in OA@INAF	2021-01-08T16:11:19Z
Title	Deep ATCA and VLA Radio Observations of Short-GRB Host Galaxies. Constraints on Star Formation Rates, Afterglow Flux, and Kilonova Radio Flares
Authors	þÿKlose, S.; Nicuesa Guelbenzu, A. M.; MichaBowski, M Hartmann, D. H.; et al.
DOI	10.3847/1538-4357/ab528a
Handle	http://hdl.handle.net/20.500.12386/29625
Journal	THE ASTROPHYSICAL JOURNAL
Number	887

The Astrophysical Journal, 887:206 (16pp), 2019 December 20 https://doi.org/10.3847/1538-4357/ab528a
© 2019. The American Astronomical Society. All rights reserved.

Deep ATCA and VLA Radio Observations of Short-GRB Host Galaxies. Constraints on Star Formation Rates, Afterglow Flux, and Kilonova Radio Flares

S. Klose[1], A. M. Nicuesa Guelbenzu[1], M. J. Michałowski[2,3], L. K. Hunt[4], D. H. Hartmann[5], J. Greiner[6], A. Rossi[7,8], E. Palazzi[7], and S. Bernuzzi[9]

[1] Thüringer Landessternwarte Tautenburg, Sternwarte 5, D-07778 Tautenburg, Germany
[2] Astronomical Observatory Institute, Faculty of Physics, Adam Mickiewicz University, ul. Słoneczna 36, 60-286, Poznań, Poland
[3] Scottish Universities Physics Alliance (SUPA), Institute for Astronomy, University of Edinburgh, Royal Observatory, Blackford Hill, EH9 3HJ, Edinburgh, UK
[4] INAF—Osservatorio Astrofisico di Arcetri, I-50125 Firenze, Italy
[5] Department of Physics and Astronomy, Clemson University, Clemson, SC 29634, USA
[6] Max-Planck-Institut fü r extraterrestrische Physik, D-85748 Garching, Germany
[7] INAF—Osservatorio di Astrofisica e Scienza dello Spazio, via Piero Gobetti 93/3, I-40129 Bologna, Italy
[8] INAF—Osservatorio Astronomico di Roma, via Frascati 33, I-00040 Monte Porzio Catone, Italy
[9] Theoretisch-Physikalisches Institut, Friedrich-Schiller-Universität Jena, D-07743, Jena, Germany
Received 2019 May 20; revised 2019 October 25; accepted 2019 October 25; published 2019 December 19

Abstract

We report the results of an extensive radio-continuum observing campaign of host galaxies of short gamma-ray bursts (GRBs). The goal of this survey was to search for optically obscured star formation, possibly indicative of a population of young short-GRB progenitors. Our sample comprises the hosts and host-galaxy candidates of 16 short-GRBs from 2005 to 2015, corresponding to roughly one-third of the presently known ensemble of well-localized short bursts. Eight GRB fields were observed with ATCA (at 5.5 and 9.0 GHz), and eight fields with the VLA (mostly at 5.5 GHz). The observations typically achieved a $1\sigma_{\rm rms}$ of 5–8 μJy. In most cases, they were performed years after the corresponding burst. No new short-GRB host with optically obscured star formation was found. Only one host galaxy was detected: that of GRB 100206A at $z = 0.407$. However, its starburst nature was already known from optical/IR data. Its measured radio flux can be interpreted as being due to a star formation rate of about $60\,M_\odot\,{\rm yr}^{-1}$. This is in good agreement with earlier expectations based on the observed broad-band spectral energy distribution of this galaxy. The 15 nondetections constrain the SFRs of the suspected host galaxies and provide upper limits on late-time luminosities of the associated radio afterglows and predicted kilonova radio flares. The nondetection of radio emission from GRB explosion sites confirms the intrinsically low luminosity of short-GRB afterglows and places significant constraints on the parameter space of magnetar-powered radio flares. Luminous radio flares from fiducial massive magnetars have not been found.

Unified Astronomy Thesaurus concepts: Gamma-ray bursts (629); Transient sources (1851); High energy astrophysics (739)

1. Introduction

The last 20 years have seen a revolution in gamma-ray burst (GRB) science, driven by new dedicated satellite missions, a deeper theoretical understanding of stellar explosions, and substantial efforts in sophisticated world-wide observing campaigns. On the one hand, long GRBs, which represent about 90% of all well-localized bursts, have been found to originate in the collapse of very massive stars (e.g., Woosley & Bloom 2006; Hjorth & Bloom 2012; Cano 2016). On the other hand, the link of short GRBs to merging compact stars was unambiguously confirmed by the gravitational wave event GW170817 (e.g., Abbott et al. 2017a, 2017b; Coulter et al. 2017; Kasen et al. 2017).

To understand diversity in burst populations, host-galaxy studies are an important observational tool. Such studies have shown that long bursts appear to originate exclusively from late-type galaxies (e.g., Fruchter et al. 2006; Wainwright et al. 2007; Lyman et al. 2017), with star formation rates (SFRs) spanning a wide range from $\sim$0.01 to $>100\,M_\odot\,{\rm yr}^{-1}$ (e.g., Sokolov et al. 2001; Christensen et al. 2004; Castro Cerón et al. 2006, 2010; Fan et al. 2010; Hunt et al. 2011). Short bursts, on the other hand, arise from all morphological types of galaxies (e.g., Fong et al. 2010, 2013; Berger 2014). By the end of 2018, well-defined positions had been found for $\sim$50 short GRBs, allowing for an identification and investigation of their hosts or host-galaxy candidates (for a review, see Berger 2014). These observations show that about 3/4 of all short GRBs originated in star-forming galaxies (e.g., Leibler & Berger 2010; Fong et al. 2011, 2013; Fong & Berger 2013), with SFRs similar to what has been found for the hosts of long GRBs.

Star formation rates in GRB host galaxies (long and short) are often derived from measured emission-line fluxes in optical bands (e.g., D'Avanzo et al. 2009). However, these lines can be affected by extinction from cosmic dust. Radio observations on the other hand trace synchrotron radiation from relativistic electrons originating from supernova remnants. As the supernova rate is directly related to the star formation rate, radio-continuum observations provide an unobscured view of the star-forming activity in a galaxy over the last 10–100 Myr (e.g., Greis et al. 2017).

Consequently, in recent years radio emission of host galaxies of long GRBs has been studied, with the goal of deriving the unobscured SFR based on the measured radio-continuum flux (e.g., Berger et al. 2003; Stanway et al. 2010; Hatsukade et al. 2012; Michałowski et al. 2012; Perley & Perley 2013; Perley et al. 2015). In a comprehensive analysis, Greiner et al. (2016) list 61 long-GRB host galaxies at redshifts $0.01 \lesssim z \lesssim 2.5$ that have been observed in the radio band. Among these, 18 were

detected and 12 (i.e., ∼20%) have a radio-derived SFR larger than $20\,M_\odot\,\mathrm{yr}^{-1}$.

Given these results for long-GRB host galaxies, the identification of three star-bursting hosts among the relatively small short-GRB ensemble (GRB 100206A, GRB 120804A, GRB 071227: Perley et al. 2012; Berger et al. 2013b; Nicuesa Guelbenzu et al. 2014, respectively) deserves attention. More such cases could be indicative of a population of young merger systems (neutron star–neutron star, neutron star–black hole) associated with short GRBs, as predicted by some stellar population synthesis models (Voss & Tauris 2003; Belczynski et al. 2006, 2007, 2018; Kruckow et al. 2018; Mapelli et al. 2018). Indeed, a general existence of young merger systems has been observationally supported by the discovery of the galactic NS–NS binary PSR J0737−3039 which will merge within only ∼85 Myr (Burgay et al. 2003; Tauris et al. 2017).

With this motivation in mind, we describe the results of a comprehensive radio-continuum study of star-forming hosts (and host-galaxy candidates; e.g., Giacomazzo et al. 2013; Berger 2014) of 16 short GRBs.[10] This is roughly one-third of all well-localized short bursts. The observations were performed using NSF's Karl G. Jansky Very Large Array (VLA) and the Australia Telescope Compact Array (ATCA).

In the following, we adopt a flat ΛCDM cosmology with Hubble constant $H_0 = 68\,\mathrm{km\,s^{-1}\,Mpc^{-1}}$ and density parameters $\Omega_M = 0.31$ and $\Omega_\Lambda = 0.69$ (Planck Collaboration et al. 2016). For the observed flux density, F_ν, we use the convention $F_\nu \sim \nu^{-\beta}$, where ν is the frequency and β is the spectral slope (in energy space, not photon number space).

2. Target Selection

Short GRBs were selected according to the compilations in Kann et al. (2011) and Berger (2014), supplemented by the database maintained by one of us (J.G.)[11] One controversial case was added to our list of short bursts (GRB 100816A, $T_{90} = 2.9 \pm 0.6$ s; see the Appendix).

Following the approach in Nicuesa Guelbenzu et al. (2014, 2015), in our radio survey we focused on a search for optically obscured star-forming activity in short-GRB hosts. We excluded events securely categorized as having early-type hosts, as in these cases we did not expect a detectable radio emission due to star-forming activity. In doing so, our first reference concerning the host-galaxy classification was the list of short-GRB host galaxies provided by Berger (2014), which contains events until mid 2013 (his Table 2). We updated this list if additional imaging data were available that required to reconsider the original classification of a host (see the Appendix). Concerning short GRBs not listed in Berger (2014), we made use of publicly available data or performed our own observations to classify suspected host galaxies. Cases with no clear host-galaxy classification (early- or late-type galaxy) were not rejected. This concerned two events (GRB 090621B and 101224A). Once this step was done, our first choice were short-GRB hosts that were detected in the infrared bands by the *Wide-field Infrared Survey Explorer* (*WISE*) satellite (Wright et al. 2010), but which are not elliptical galaxies. Cases with more than one host-galaxy candidate were included in our target list as long as at least one candidate is not an elliptical galaxy. Radio observations could in principle reveal if one host-galaxy candidate is special in some sense, e.g., exhibits a high SFR.

WISE observed the entire sky in four bands at 3.4, 4.6, 12, and 22 μm (*W1, W2, W3, W4*; see Wright et al. 2010). The *WISE* catalog[12] lists all sources with a measured signal-to-noise ratio greater than five in at least one band. Even though the catalog does not have the same sensitivity in all directions, for our purpose it was the best available infrared all-sky database.

Our analysis showed that 12 short-GRB host galaxies were detected by *WISE* in at least one band (Table 1). This is ∼1/3 of the sample of short-GRB hosts (by the year 2015). No host galaxy has been detected at the longest wavelength (*W4*), while five hosts were detected in the *W1, W2*, and *W3* bands: GRB 060502B at $z = 0.287$, GRB 071227 at $z = 0.381$, GRB 100206A at $z = 0.407$, GRB 150101B at $z = 0.134$, and GRB 161104A with an unknown z. It is noteworthy that these are not the cosmologically nearest short-GRB hosts. According to their position in the *WISE* color–color diagram, which combines the *W1–W2* color with the *W2–W3* color (Wright et al. 2010, their Figure 12), the hosts of GRB 071227 and 100206A fall into the starburst category. Similarly, the host of GRB 060502B might be a spiral, while the hosts of GRB 150101B and 161104A could be elliptical galaxies. (See also Fong & Chornock 2016; Fong et al. 2016a; Xie et al. 2016.) Moreover, the host of GRB 150101B is the first GRB host galaxy that harbors an AGN (Xie et al. 2016).

A subset of six host galaxies (or host-galaxy candidates) were detected by *WISE* in *W1* and *W2* but not in *W3* and *W4*, while two hosts have only a detection in filter *W1*. The former group includes GRB 050724, 070724, 070729, 111222A, 130603B, and 150424A, the latter group GRB 070429B and 100816A. Among these, the field of GRB 070729 contains several host-galaxy candidates. Unfortunately, no redshift is known in this case.

Additional targets were selected according to redshift, because for sensitivity considerations, we wanted to include nearby hosts if possible; thus, an additional group of five targets entered our list because of their redshift ($z < 0.5$), even though they were not seen by *WISE* in any band (GRB 061006, 061201, 061210A, 070809, and 080123).

Finally, we observed three additional short-GRB hosts with unknown redshifts (GRB 090621B, 101224A, and 130515A). The common trait of these hosts is that there was no optically detected transient. The status of the identification of their host galaxies is thus very different, ranging from "no known host-galaxy candidate" (GRB 090621B) to "a host-galaxy candidate outside the *Swift*/XRT error circle" (GRB 130515A). If they were dusty star-bursting galaxies similar to the host of the short GRB 120804A (SFR $\sim 300\,M_\odot\,\mathrm{yr}^{-1}$; Berger et al. 2013b), we would have been able to detect them up to a redshift $z \sim 1.5$.

Altogether, our sample consists of 16 short-GRB host galaxies which span a redshift range from $z = 0.1$ to 0.8 (Table 2). According to Bromberg et al. (2013) (see also Wanderman & Piran 2015), bursts with $T_{90} < 0.8$ s represent a much cleaner short-burst sample than longer short-GRB events. Most of our targets belong to this $T_{90} < 0.8$ s category, i.e., based on their duration these events are confidently a merger and not a collapsar.

[10] Host-galaxy candidates have no secure association with the burst under consideration, but are selected according to a chance coincidence analysis given their apparent magnitude in a certain photometric band and their angular offset from the burst position (Bloom et al. 2002).

[11] http://www.mpe.mpg.de/~jcg/grbgen.html.

[12] http://wise.ssl.berkeley.edu/

Table 1
Host Galaxies of Short GRBs (by 2015) in the *WISE* Satellite Archive (all-sky)

GRB (1)	Decl. (2)	*W1* (3)	*W2* (4)	*W3* (5)	*W4* (6)	*W1–W2* (7)	*W2–W3* (8)	Gal. Type (9)
050724	−27	15.35 ± 0.05	15.41 ± 0.13	>12.37	>8.42	−0.06 ± 0.14	<3.04 ± 0.13	
060502B	+52	15.29 ± 0.03	14.94 ± 0.04	12.88 ± 0.35	>9.65	0.35 ± 0.05	2.06 ± 0.35	Spiral
070429B	−32	17.38 ± 0.15	>16.68	>12.44	>9.01	<0.70 ± 0.15	⋯	
070724	−18	17.03 ± 0.11	16.37 ± 0.22	12.34 ± 0.37	>9.13	0.66 ± 0.25	4.03 ± 0.43	
070729	−39	16.54 ± 0.05	16.69 ± 0.18	>13.22	>9.34	−0.15 ± 0.19	<3.47 ± 0.18	
071227	−55	15.58 ± 0.03	15.15 ± 0.05	11.88 ± 0.16	>9.70	0.43 ± 0.06	3.27 ± 0.17	LIRG
100206A	+13	15.71 ± 0.05	15.15 ± 0.10	11.31 ± 0.18	>8.57	0.56 ± 0.11	3.84 ± 0.21	LIRG
100816A	+26	17.08 ± 0.12	16.87 ± 0.36	>12.05	>8.79	0.21 ± 0.38	<4.82 ± 0.36	
111222A	+65	13.26 ± 0.02	13.16 ± 0.03	>12.45	>8.91	0.10 ± 0.04	<0.71 ± 0.03	
130603B	+17	17.05 ± 0.11	16.95 ± 0.37	>12.53	>8.91	0.10 ± 0.39	<4.42 ± 0.37	
150101B	−10	13.43 ± 0.03	13.18 ± 0.03	12.39 ± 0.48	>8.78	0.25 ± 0.04	0.79 ± 0.48	Elliptical
150424A	−26	16.44 ± 0.07	16.10 ± 0.17	>12.12	>8.69	0.34 ± 0.18	<3.98 ± 0.17	

Note. Listed here are all short-GRB hosts and host-galaxy candidates with detections in at least one of the four *WISE* bands (Wright et al. 2010). Upper limits are given according to the *WISE* catalog. Column #2 gives the decl. (J2000) in degrees (which decides between a potential ATCA or VLA target), columns #3–#6 the magnitudes on the four *WISE* bands, and columns #7 and #8 the corresponding *W1–W2* and *W2–W3* color (in mag), respectively, which enters the *WISE* color–color diagram and provides the type of the galaxy (column #9; LIRG = Luminous Infrared Galaxy). All magnitudes refer to the Vega photometric system.

Table 2
Target List

GRB (1)	Select. (2)	z (3)	R.A. (J2000) (4)	Decl. (5)	Position (6)	T_{90}(s) (7)
ATCA						
050724	*WISE*	0.258	16:24:44.36	−27:32:27.5	OT	3.0 ± 1.0
061006	redshift	0.4377	07:24:07.66	−79:11:55.1	OT	0.42
061201	redshift	0.111	22:08:32.09	−74:34:47.1	OT	0.8 ± 0.1
070729	*WISE*		03:45:15.97	−39:19:20.5	XRT	0.9 ± 0.1
070809	redshift	0.2187	13:35:04.55	−22:08:30.8	OT	1.3 ± 0.1
080123	redshift	0.496	22:35:46.33	−64:54:02.7	XRT	0.4
130515A	noOT		18:53:45.71	−54:16:45.5	XRT	0.29 ± 0.06
150424A	*WISE*	0.2981	10:09:13.38	−26:37:51.5	OT	0.4
VLA						
060502B	*WISE*	0.287	18:35:44.97	52:37:52.4	XRT	0.09 ± 0.02
061210	redshift	0.4095	09:38:05.17	15:37:17.5	XRT	0.047
070724A	*WISE*	0.457	01:51:14.07	−18:35:39.3	OT	0.4 ± 0.04
090621B	noOT		20:53:53.16	69:01:41.5	XRT	0.14 ± 0.04
100206A	*WISE*	0.4068	03:08:39.00	13:09:24.8	XRT	0.12 ± 0.03
100816A	*WISE*	0.8049	23:26:57.56	26:34:42.9	OT	2.9 ± 0.6
101224A	noOT		19:03:41.72	45:42:49.5	XRT	0.20 ± 0.01
130603B	*WISE*	0.3565	11:28:48.15	17:04:18.0	OT	0.18 ± 0.02

Note. Column #2 classifies the used selection criteria: (i) *WISE* all-sky survey, (ii) small redshift, or (iii) no detected optical transient (noOT; see Section 2). Column #3 provides the redshift (see the Appendix), if available. Columns #4 and #5 either give the position of the OT or the central coordinates of the XRT error circle (http://www.swift.ac.uk/xrt_positions/; Goad et al. 2007; Evans et al. 2009) as of 2019 January. Column #6 distinguishes between the OT and the XRT position of the afterglow. Column #7 provides the burst duration T_{90}, mostly measured in the *Swift*/BAT energy band (15–350 keV). For references see the Appendix.

3. Observations and Data Reduction

3.1. Radio Data

All radio-continuum observations were performed with ATCA and VLA in the years 2013–2015.

ATCA observations were carried out in the 5.5 and 9.0 GHz bands (corresponding to 6 and 3 cm, respectively), using the upgraded Compact Array Broadband Backend (CABB) detector (Wilson et al. 2011) and all six 22-m antennae with the 6 km baseline (Table 3; programme ID C2840, PI: A. Nicuesa Guelbenzu). We set a technical observing constraint of decl. (J2000) $< -15°$. ATCA can achieve a sensitivity at 5.5 GHz of $\sigma_{\rm rms} \sim 5\,\mu$Jy beam^{-1} in a $\sim$10 hr integration. Therefore, whenever possible we stayed on a target between 10 and 12 hr to obtain the deepest sensitivity, as well as the best coverage of the *uv* plane for image fidelity. The 5.5 GHz band is a good compromise between sensitivity and expected radio flux on the one hand, and relatively lower radio frequency interference (RFI) on the other. In the observing mode used here, CABB integrates at 5.5 and 9.0 GHz simultaneously, each with 2048 spectral channels of width 1.0 MHz.

Observations with the VLA went similarly deep as those with ATCA, with integration times typically a factor of 10 smaller because of the larger number of antennas. Observations were performed via dynamical scheduling (programme ID 13B-313, 14B-201, 15B-214; PI: A. Nicuesa Guelbenzu). Most data were

Table 3
Summary of the Radio Observations

GRB (1)	Date Obs. (2)	Config. (3)	Time (4)	Flux Calib. (5)	Phase Calib. (6)	Freq. (7)	Beam Size (8)	$1\sigma_{\rm rms}$ (9)
ATCA								
050724	2015 Oct 23	6A	10.4	0823–500	1622–253	5.5	4.4 × 1.5	5.0
						9.0	2.7 × 0.9	5.2
061006	2013 Jul 20	6A	7.0	1934–638	0637–752	5.5	3.0 × 1.3	7.8
						9.0	1.9 × 0.8	9.3
061201	2013 Jul 21	6A	11.5	0823–500	2142–758	5.5	2.3 × 1.5	5.2
						9.0	1.4 × 0.9	5.2
	2013 Jul 26	6A	3.2	1934–638	2142–758	5.5,9.0		
	2013 Jul 25	6A	0.7	1934–638	2142–758	5.5,9.0		
070729	2015 Apr 28	6A	11.0	0823–500	1934–638	5.5	4.5 × 2.5	7.3
						9.0	2.7 × 1.5	6.9
070809	2013 Jun 19	6A	9.5	1934–638	1308–220	5.5	7.7 × 1.7	6.0
						9.0	4.7 × 1.1	6.4
080123	2013 Jul 25	6A	8.7	1934–638	2353–686	5.5	2.6 × 1.5	6.4
						9.0	1.6 × 0.9	6.6
130515A	2015 Oct 26	6A	7.1	1934–638	1824–582	5.5	3.6 × 1.3	6.2
						9.0	2.2 × 0.8	7.3
150424A	2015 Jun 19	6D	1.8	1934–638	1034–293	5.5	12.0 × 1.5	7.1
						9.0	7.0 × 0.9	8.0
	2015 Oct 23	6A	3.2	0823–500	1034–293	5.5,9.0		
VLA								
060502B	2014 Jan 18	B	0.75	3C286	J1829+4844	3.0	3.0 × 2.0	8.8
	2014 Oct 09	C	1.0	3C286	J1740+5211	5.5	4.0 × 3.4	6.4
061210	2014 Oct 16	C	1.0	3C286	J0854+2006	5.5	3.7 × 3.2	5.3
070724A	2014 Sep 19	DnC	1.5	3C147	J0204–1701	5.5	11.2 × 7.0	7.6
090621B	2015 Oct 08	D	0.75	3C286	J2022+6136	5.5	16.2 × 10.6	5.7
	2015 Oct 17	D	0.5	3C286	J2022+6136	5.5		
	2015 Oct 24	D	0.5	3C286	J2022+6136	5.5		
	2015 Oct 28	D	0.5	3C147	J2022+6136	5.5		
100206A	2014 Oct 10	C	1.5	3C147	J0318+1628	5.5	4.0 × 3.9	13
100816A	2014 Oct 9	C	1.5	3C147	J2340+2641	5.5	5.8 × 3.8	5.8
101224A	2015 Oct 12	D	0.5	3C286	J1845+4007	5.5	11.2 × 10.0	6.4
	2015 Oct 14	D	0.75	3C48	J1845+4007	5.5		
	2015 Oct 20	D	0.75	3C286	J1845+4007	5.5		
	2015 Oct 27	D	0.75	3C48	J1845+4007	5.5		
	2015 Oct 30	D	0.75	3C286	J1845+4007	5.5		
130603B	2014 Nov 13	C	1.5	3C286	J1120+1420	5.5	3.9 × 3.5	6.5

Note. Column #2 provides the date of the start of the observations, column #3 gives the telescope configuration. Column #4 provides the telescope time (in hr). Columns #5 and #6 list the flux and phase calibrators, column #7 the effective frequency. The last two columns contain the size of the synthesized beam in units of arcsec and the 1σ rms of the resulting image (in units of μJy beam^{-1}; measured using the `imstat` task under MIDAS and CASA, respectively). Beam sizes and the rms refer to a robust parameter of 0.5. Except for the *S*-band (3 GHz) observations of the host of GRB 060502B on 2014 January 18, all VLA observations were performed in the *C* band (effectively at 5.5 GHz). For GRB 061201, 090621B, 101224A, and 150424A the 1σ rms and beam size refer to the combined data set.

obtained in the *C* band (effectively at 5.5 GHz) in C or D telescope array configuration. One target was also observed in the *S* band in B configuration (effectively at 3.0 GHz; Table 3). All VLA observations used the WIDAR correlator with the wideband setup and the 8-bit samplers. They were performed in 16 spectral windows with a bandwidth of 128 MHz each, providing a total bandwidth of 2048 MHz per polarization.

In principle, observations in the 2.1 GHz band (16 cm) could provide a better signal-to-noise ratio, because for star-forming galaxies the radio flux typically scales as $F_\nu \propto \nu^{-\beta}$, $\beta \sim 0.7$ (e.g., Gioia et al. 1982; Tabatabaei et al. 2017; Klein et al. 2018). However, this band is more affected by RFI. In addition, source crowding at 2.1 GHz is higher, making the identification of faint radio sources more challenging. Moreover, compared with observations in the 2.1 GHz band, at 5.5 GHz the radio sky is less populated with bright radio sources, which can also affect the image reconstruction.

During the observations, bandpass and flux calibration were performed in the usual manner. For ATCA observations in most cases the bright radio source PKS 1934–638 (R.A., decl. J2000 = 19:39:25.026, −63:42:45.63) was used as the calibrator. If this source was not observable, then 0823–500 was observed (R.A., decl. J2000 = 08:25:26.869, −50:10:38.49). For VLA, the bright radio sources 3C286, 3C147, and 3C48 were observed. Nearby calibrators for phase referencing were chosen depending on the target coordinates via the corresponding web interface provided by the ATCA and the VLA operating institutes CSIRO and NRAO, respectively.[13]

Data reduction was performed with the standard software packages. ATCA data were reduced using the Multichannel Image Reconstruction, Image Analysis and Display (MIRIAD)

[13] For the coordinates and fluxes of the ATCA phase calibrators, see https://www.narrabri.atnf.csiro.au/calibrators/c007/atcat.html.

software package version 1.5 (Sault et al. 1995); for VLA we used the data reduction pipeline under CASA version 5.1.2-4. During the data processing, RFI was examined and eliminated as well as possible from the data. All data were Fourier-transformed using the Briggs robust weighting option (Briggs 1995), varying this parameter between 0.5, 1.0, and 2.0, and selecting the one that gave the best compromise between the resolution and the noise.

Usually, targets were observed for ∼7–11 hr (ATCA) and 1–2 hr (VLA) of elapsed telescope time. Consequently, all observations are fairly deep, typically reaching a $1\sigma_{\rm rms}$ between 5 and 8 μJy beam^{-1} (measured in an empty field around the target position). For 11 of the 16 targets the resulting synthesized beam size was smaller than 5×5 arcsec^2. Observing parameters are reported in Table 3.

3.2. Optical Data

Imaging. Optical/near-infrared (NIR) data was downloaded from public data archives (ESO/VLT, Gemini, GTC, *HST*). Multi-color data were obtained using the optical/NIR seven-channel imager GROND mounted at the 2.2 m ESO/MPG telescope on ESO/La Silla (Chile) (Greiner et al. 2007, 2008). In two cases (GRB 100816A, 150424A), the optical SFR was also estimated based on a `Le Phare`[14] (Arnouts et al. 1999; Ilbert et al. 2006; Arnouts et al. 2013) analysis of the broad-band spectral energy distribution (SED) of the galaxy.

Spectroscopy. In the majority of cases, the optical SFR was taken from the literature and is based on emission-line spectroscopy. In two cases the optical SFR was derived either by using our own data (GRB 080123) or by a reanalysis of archival data (GRB 150424A) using the equations relating [H II] luminosity and SFR published in Kennicutt (1998) and Savaglio et al. (2009). Additional details on individual targets are provided in the Appendix. If not otherwise stated, SFR measurements based on emission-line spectroscopy were not corrected for host-galaxy extinction, slit losses were usually taken into account.

4. Results

4.1. Radio Detection of the Host of GRB 100206A

With our deep radio observations, we detected only one target in our sample: the suspected host of GRB 100206A (Table 2). Using the `imfit` task under CASA, at 5.5 GHz we measure a flux density of $F_\nu = 65 \pm 11$ μJy, centered at R.A., decl. (J2000) = 03:08:39.148 ± 0.017 s, 13:09:29.28 ± 0.″15. The flux we measure from this source is in agreement with its reported nondetection by Berger et al. (2013b), who found $F_\nu(5.8\,{\rm GHz}) \lesssim 80$ μJy (5σ).

The radio centroid (positional error ∼0.″2) lies 5″ away from the center of the *Swift*/XRT 90% c.l. error circle, which at $z = 0.4068$ corresponds to a projected spatial distance of ∼30 kpc. It coincides with the bulge of the suspected GRB host galaxy (G1; Figure 1). Assuming a Gaussian distribution for XRT position measurements, this angular distance excludes the origin of the X-rays from the position of the radio centroid with 99% probability. Conversely, with high confidence we do not detect (Table 3) radio emission from sources inside the XRT error circle. Therefore, it is unlikely that the measured radio flux is physically related to the burst (e.g., the radio afterglow).

[14] http://www.cfht.hawaii.edu/~arnouts/LEPHARE/lephare.html

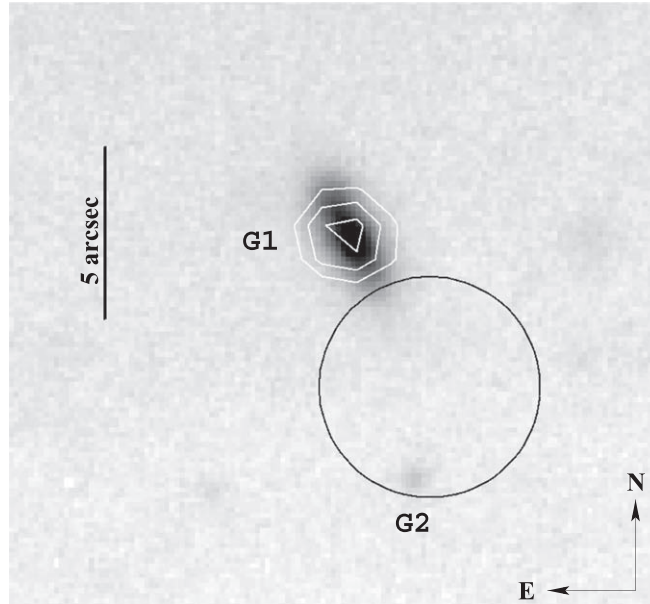

Figure 1. Radio 5.5 GHz flux contours superimposed on a Gemini-N/GMOS *i*-band image of the field of GRB 100206A (programme ID GN-2010A-Q-7, PI: D. Perley). The XRT error circle (90% c.l.; see the Appendix) is shown (radius 3.″2; as of 2019 January), together with the suspected host galaxy (G1), and a fainter galaxy (G2) inside the error circle. Radio contour lines shown in white correspond to 3, 3.5, and 4 times the local $1\sigma_{\rm rms}$ (Table 3). At the redshift of GRB 100206A, 1″ corresponds to 5.6 kpc projected distance.

Furthermore, according to Perley et al. (2012) the observed [N II]/Hα and [O III]/Hβ emission-line ratios of this galaxy favor the interpretation that the strong Hα line is due to star formation and not associated with AGN activity. This would be consistent with evidence from the radio map; using the `imfit` task under CASA, the radio source is marginally resolved in one direction which would be unexpected in the case of an AGN.

In order to calculate the radio SFR, we follow Greiner et al. (2016) (with reference to Murphy et al. 2011), according to which[15]

$$\frac{{\rm SFR_{Radio}}}{M_\odot\,{\rm yr}^{-1}} = 0.059\left(\frac{F_\nu}{\mu{\rm Jy}}\right)(1+z)^{(\beta-1)}\left(\frac{d_L}{\rm Gpc}\right)^2\left(\frac{\nu}{\rm GHz}\right)^\beta. \quad (1)$$

Here, d_L is the luminosity distance, β is the spectral slope (unlike those authors, we use the convention $F_\nu \sim \nu^{-\beta}$).

If the observed radio flux is completely due to star-forming activity, then it corresponds to a SFR of $59 \pm 10\,M_\odot\,{\rm yr}^{-1}$ (assuming $\beta = 0.7$). This is roughly twice the value derived by Perley et al. (2012) from a study of the broad-band SED of this galaxy in the wavelength range between ∼0.5 and 20 μm (observer frame).

This picture does not change when we perform a GRASIL analysis of the SED of this galaxy from the optical to the radio band,[16] analogous to what we have done in Nicuesa Guelbenzu et al. (2014). Adding now the radio detection to the data implies a SFR of $63\,M_\odot\,{\rm yr}^{-1}$, an IR luminosity of $\log(L_{\rm IR}/L_\odot) = 11.58$, a mass in stars of $\log(M_\star/M_\odot) = 11.42$, and a global host visual extinction of $A_V = 2.10$ mag.

[15] For a recent discussion on the radio-based SFR calibration, we refer to the comprehensive analysis by Tabatabaei et al. (2017), Mahajan et al. (2019), and Tisanić et al. (2019).

[16] For details of the code and the set of templates, see Silva et al. (1998), Iglesias-Páramo et al. (2007), and Michałowski et al. (2010).

Recently, Perley et al. (2017) reported results of a reobservation of several long-GRB host galaxies where substantial radio-derived star formation rates in excess of $100\,M_\odot\,\mathrm{yr}^{-1}$ had been found in previous studies. Surprisingly, these authors could not reproduce the previously reported large SFRs for any of their five hosts. As stressed by Perley et al. (2017), radio afterglow contamination, noise fluctuations, and numerical artifacts produced by the image processing could have affected some of the previous radio detections. In the case of GRB 100206A, our detection and radio flux measurement is supported by three independent studies: the flux density we measure at 5.5 GHz fits well with what has been predicted for this galaxy based on its observed optical/infrared broad-band SED (Perley et al. 2012; Nicuesa Guelbenzu et al. 2014, their Figure 4; Contini 2018, her Figure 3).

Even though the host of GRB 100206A is forming stars at a high rate, a physical link between the formation of the GRB progenitor to the present epoch of star formation cannot be established. Though the (90% c.l.) XRT error circle touches the outer regions of the suspected host galaxy (G1, Figure 1), the large (projected) spatial offset between the burst position and the centroid of the detected radio source disfavors such a conclusion.

4.2. Nondetections and Upper Limits on Star Formation Rates

For the remaining 15 targets, we can only provide deep upper limits on the SFR, as given in Table 4. In the case of our ATCA observations the SFR is best constrained at 5.5 GHz. In the case of VLA all limits on the SFR refer to observations in the C band (5.5 GHz).

Figure 2 summarizes the radio-derived SFRs.[17] For those cases in our target list where more than one host-galaxy candidate is implicated, we only plot the result for the host-galaxy candidate with the smallest redshift (in no cases is this an elliptical galaxy). The four bursts from our sample without spectroscopic redshifts (GRB 070729, 090621B, 101224A, and 130515A) are not plotted. These data are supplemented by data taken from Nicuesa Guelbenzu et al. (2014; GRB 071227), and Berger et al. (2013b; GRB 120804A). In addition, we display data from Fong et al. (2015, their Table 8) and Fong et al. (2016b, their Table 1). All upper limits reported by these authors have been transformed to an observing frequency of 5.5 GHz, assuming a spectral slope $\beta = 0.7$. In those cases where several observations with different upper limits were reported for the same host, only the most constraining data point is plotted.[18]

Figure 2 shows that at 5.5 GHz a sensitivity of better than about 40 μJy (5σ rms) has been reached for more than 50% of the targeted galaxies. Reaching much deeper sensitivity limits would require much more telescope time.

If we consider a SFR sensitivity of $20\,M_\odot\,\mathrm{yr}^{-1}$ as a minimum we would like to achieve for a target, then we are restricted to the lowest redshifts, $z \lesssim 0.3$. In our sample all 5 targeted galaxies in this redshift range remained undetected. For the nearest events at $z < 0.2$ the inferred SFR upper limits do even reach 1.5–5 $M_\odot\,\mathrm{yr}^{-1}$. Though the sample size is small, one important result can be stressed: in no case evidence for intense star-forming activity close to a GRB explosion site has been found.

Going to higher redshifts increases the sample size, but already for targets with $z \gtrsim 0.5$ the achieved SFR sensitivity is just sufficient to potentially find the most extreme star-forming hosts: At redshifts $z \gtrsim 0.5$ even star-forming galaxies with a SFR of $\sim 50\,M_\odot\,\mathrm{yr}^{-1}$ will not be detected anymore. All this naturally limits the meaningfulness of such radio surveys.

Nevertheless, the data clearly show that the majority of short-GRB hosts is not forming stars at a high rate, though some clearly do. This raises the question whether the percentage of heavily star-forming hosts among the short-GRB host-galaxy ensemble is unexpectedly high.

Table 4
Radio-derived Star formation Rates

GRB	z	SFR(radio) ($M_\odot\,\mathrm{yr}^{-1}$)	SFR(opt.) ($M_\odot\,\mathrm{yr}^{-1}$)	References
ATCA				
050724	0.258	<8	<0.05–0.17	(1)
061006	0.438	<42	0.02	(2)
061201	0.111	<1.5	0.14	(3)
070729	0.8	<160		
070809	0.219	<7	0.15	(4)
080123	0.496	<46	0.7	(5)
130515A	0.5	<45		
150424A	0.298	<16	0.5–7	(5)
VLA				
060502B	0.287	<12	0.4–0.8	(6)
061210	0.410	<25	1.2	(6)
070724A	0.457	<45	8.4 (+0.6,−6.1)	(11)
090621B	0.5	<42		
100206A	0.407	59 ± 10	30	(8)
100816A	0.805	<127	58^{+51}_{-26}	(7)
101224A	0.5	<47		
130603B	0.356	<22	1.7–5	(6), (9)

Note. Radio-derived upper limits refer to $5\sigma_{\mathrm{rms}}$ at 5.5 GHz (Equation (1)). In three cases no redshift is known and we assumed $z = 0.5$; for GRB 070729 we used a photometric redshift estimate from Leibler & Berger (2010; see the Appendix). If not otherwise stated, optical data refer to emission-line measurements. See the Appendix for more details. Additional notes to individual sources: GRB 061201: the data refer to the host-galaxy candidate G1. GRB 070809: the data refer to the host-galaxy candidate G1. The host-galaxy candidate G2 is not included in this table as it is an elliptical galaxy. GRB 100206A: the data refer to the host-galaxy candidate G1. GRB 130515A: the SFR is based on a `Le Phare` fit of the broad-band SED obtained with GROND (Figure 9). GRB 150424A: the data refer to the bright spiral next to the OT. The SFR based on optical spectroscopy is 0.15 $M_\odot\,\mathrm{yr}^{-1}$, while the SFR based on a `Le Phare` fit of the galaxy's SED is $\sim$7 $M_\odot\,\mathrm{yr}^{-1}$ (Figure 10).
References. (1) Berger et al. (2005), Prochaska et al. (2006), Malesani et al. (2007), (2) Berger (2009), (3) Stratta et al. (2007), (4) Perley et al. (2008), (5) this work, (6) Berger (2014), (7) Krühler et al. (2015), (8) Perley et al. (2012), (9) Cucchiara et al. (2013), Fong et al. (2014), de Ugarte Postigo et al. (2014), (10) Kocevski et al. (2010), (11) Chrimes et al. (2018).

4.3. The Most Actively Star-forming Short-GRB Hosts

Among the 25 short-GRB host galaxies listed in Berger (2014) which have a measured SFR (bursts from mid 2005 to

[17] A similar plot is shown in Stanway et al. (2014) but for long-GRB host galaxies. Since these authors used a slightly different equation for the transformation of radio flux into SFR, their curves SFR(z, F_ν) do not perfectly match the curves shown here. Because of analogous reasons, the radio-SFR calculated for GRB 120804A differs slightly from the SFR calculated by Berger et al. (2013b, their Equation (4)).

[18] Seven bursts in our target list are also included in the summarizing table in Fong et al. (2015). Our radio upper limits are significantly deeper, however. The field of GRB 050724, 070724A, and 130603B was also observed with the VLA by Fong et al. (2016b); their upper limits agree with ours.

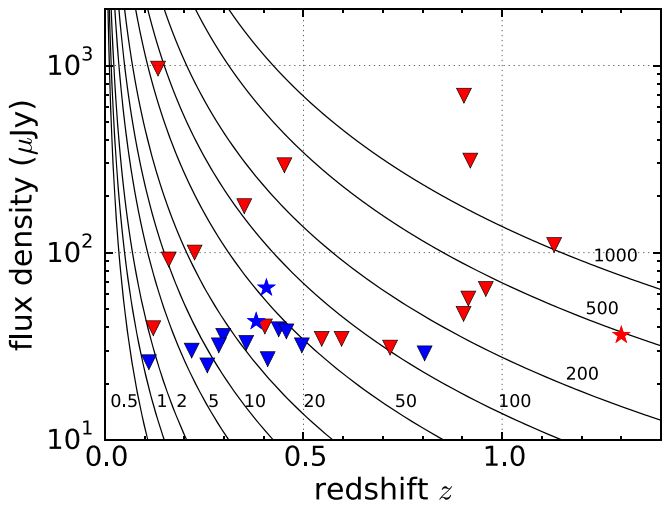

Figure 2. Radio-continuum flux at 5.5 GHz from short-GRB host galaxies and the corresponding radio-derived star formation rates (Equation (1)). Color coding: blue is from this work (Table 4), as well as GRB 071227 (Nicuesa Guelbenzu et al. 2014), red is data from Fong et al. (2015, 2016b). Detections are shown as stars (GRB 071227, 100206A, and 120804A), $5\sigma_{\rm rms}$ upper limits as downwards pointing triangles. Solid lines correspond to different star formation rates (in units of $M_\odot\,{\rm yr}^{-1}$).

2010), 18 hosts have an optical SFR $\lesssim 2.5\,M_\odot\,{\rm yr}^{-1}$ (in his list GRB 071227 has $0.6\,M_\odot\,{\rm yr}^{-1}$). The remaining seven hosts have an optical SFR between 2.5 and $30\,M_\odot\,{\rm yr}^{-1}$. Only the host of GRB 100206A (in his list $30\,M_\odot\,{\rm yr}^{-1}$) and GRB 101219A ($16\,M_\odot\,{\rm yr}^{-1}$) lie above $10\,M_\odot\,{\rm yr}^{-1}$.

Following GRB 071227 (Nicuesa Guelbenzu et al. 2014), the host of GRB 100206A is the second short-GRB host in our sample with a radio detection due to star formation activity. Together with the hosts of GRB 101219A ($z = 0.718$; Chornock & Berger 2011), GRB 100816A (see Table 4; Krühler et al. 2015), and GRB 120804A (SFR $\sim 300\,M_\odot\,{\rm yr}^{-1}$, $z \sim 1.3$; Berger et al. 2013b), these five hosts represent the current sample of very actively star-forming galaxies that hosted a short GRB (SFR $> 10\,M_\odot\,{\rm yr}^{-1}$). Though the sample size of these very actively star-forming galaxies is small, it represents at least $\sim$10% of the short-GRB host-galaxy population (including all morphological types of hosts).

Given this percentage, is this pointing to a subpopulation of young NS–NS merger systems which were born in recent starbursts? When exploring the consequences of the discovery of the heavily star-forming hosts of GRB 100206A and GRB 120804A, Perley et al. (2012) and Berger et al. (2013b) pointed out that in the redshift range 0.5–1.0, i.e., close to the redshift range where massive star-forming short-GRB hosts have been found ($z \gtrsim 0.4$), the comoving number density of massive, luminous and ultra-luminous infrared galaxies accounts for 10%–20% of the total comoving SFR density of the universe (Casey et al. 2014), but only a small fraction of comoving stellar mass density (Caputi et al. 2006). In this respect, the fraction of heavily star-forming short-GRB hosts found so far is not remarkably high. Thus there is currently no evidence for a subpopulation of short-lived (young) short-GRB progenitors which were born in recent starbursts. Future multi-wavelength studies of very nearby hosts are required to address this question with better statistics.

5. Constraints on Radio Emission from Late-time Short-GRB Radiation Components

Even though our radio data were taken with the goal of searching for optically hidden star-forming activity, our nondetections are well suited to set deep constraints on late-time radiation components of short GRBs. In the following, we quantify the observational limits that can be placed on flux from late-time radio afterglows and late-time kilonova radio flares.

5.1. Constraints on Late-time Radio Afterglow Flux

In the time window we are studying here (months to years after the corresponding burst), no radio afterglow of a short GRB has ever been detected. The short burst with the latest successful radio observation is GRB 140903A, whose radio afterglow was still found $\sim$10 days post burst (Fong et al. 2015; Zhang et al. 2017). For comparison, several long-GRB radio afterglows have been successfully observed at host-frame times >100 days (Chandra & Frail 2012, their Figure 7). The most extreme example here is the long GRB 030329 whose radio afterglow was still detected several years after the burst (van der Horst et al. 2008; Peters et al. 2019).

Chandra & Frail (2012) performed a detailed analysis of 14 yr of radio follow-up observations of GRB afterglows with the VLA, including 35 short bursts (with 2 detections). These data confirmed what is known from the optical/X-ray bands (e.g., Nysewander et al. 2009; Kann et al. 2011; Nicuesa Guelbenzu et al. 2012): short-GRB afterglows are intrinsically dim sources, in each wavelength region being on average at least one order of magnitude fainter than long GRBs. According to Figure 8 in Chandra & Frail (2012), in our time window we would expect an afterglow radio luminosity at 8.5 GHz far below $10^{29}\,{\rm erg\,s^{-1}\,Hz^{-1}}$. Changing the observed frequency to 5.5 GHz does not substantially change this conclusion.

In order to calculate the k-corrected luminosities we would infer from our radio observations, we followed Chandra & Frail (2012) (note our convention for F_ν; Section 1):

$$L_\nu = 4\pi d_L^2\, F_\nu (1+z)^{\beta-1}. \quad (2)$$

Following these authors, in Table 5 the luminosity $L_{\nu,1}$ assumes an optically thin, flat, post-jet-break radio afterglow with a spectral slope $\beta = -1/3$ (i.e., a positive radio slope) while $L_{\nu,2}$ assumes a kilonova radio flare with $\beta = 0.7$ (see Section 5.2).

Table 5 presents the constraints we place on the late-time radio luminosity of the 16 short-GRB events studied here. In the case of multiple 5.5 GHz observations of the same target (GRB 061201, 090621B, 101224A) the calculated luminosities refer to the combined data set, averaged over the time of the observing runs (which were close to each other). This averaging was not done for GRB 060502B, since here the observations included two different frequencies; we used only the result for the 5.5 GHz observation in 2014 October. Finally, an averaging was not done for GRB 150424A either; here only the data from the observing run in 2015 June were taken into account (see the Appendix).

Table 5 shows that our observations achieved a sensitivity between 0.1 and $5 \times 10^{29}\,{\rm erg\,s^{-1}\,Hz^{-1}}$. Assuming that after its peak a radio afterglow flux fades according to $F_\nu \sim t^{-1}$ (Chandra & Frail 2012), our nondetection of radio emission

Table 5
Upper Limits on the Luminosities of Radio Afterglows and Late-time Radio Flares

GRB (1)	z (2)	$dt/(1+z)$ (3)	$F_\nu^{\rm lim}$ (4)	$L_{\nu,1}$ (5)	$L_{\nu,2}$ (6)	$\nu L_{\nu,1}$ (7)	$\nu L_{\nu,2}$ (8)
ATCA							
050724	0.258	8.149	25	4.0	5.0	2.2	2.8
061006	0.438	4.721	39	17.7	25.8	9.7	14.2
061201	0.111	5.979	26	0.8	0.8	0.4	0.5
070729	0.8	4.531	37	52.8	96.8	29.0	53.3
070809	0.219	4.810	30	3.4	4.2	1.9	2.3
080123	0.496	3.678	32	18.6	28.1	10.2	15.5
130515A	0.5	1.632	31	18.3	27.8	10.0	15.3
150424A	0.298	0.118	68	14.3	18.7	7.9	10.3
VLA							
060502B	0.287	5.995	44	8.7	11.2	2.6	3.4
		6.556	32	6.3	8.2	3.5	4.5
061210A	0.410	5.569	27	10.6	15.1	5.8	8.3
070724	0.457	4.912	38	18.8	27.7	10.3	15.2
090621B	0.5	4.219	29	16.8	25.5	9.2	14.0
100206A	0.407	3.322	65	25.6	36.4	14.1	20.0
100816A	0.805	2.298	29	42.4	78.0	23.3	42.9
101224A	0.5	3.215	32	18.9	28.7	10.4	15.8
130603B	0.356	1.066	33	9.8	13.5	5.4	7.4

Note. Column #2 provides the used redshift, column #3 the time after the burst in the GRB host frame in years. Column #4 lists the 5σ observed upper limits of the flux density (in μJy). The following two columns provide the specific luminosities in 10^{28} erg s^{-1} Hz^{-1} (assuming isotropic emission). The two last columns contain νL_ν in 10^{38} erg s^{-1}. $L_{\nu,1}$ assumes a radio afterglow, $L_{\nu,2}$ a kilonova radio flare (see text). All luminosities refer to 5.5 GHz.

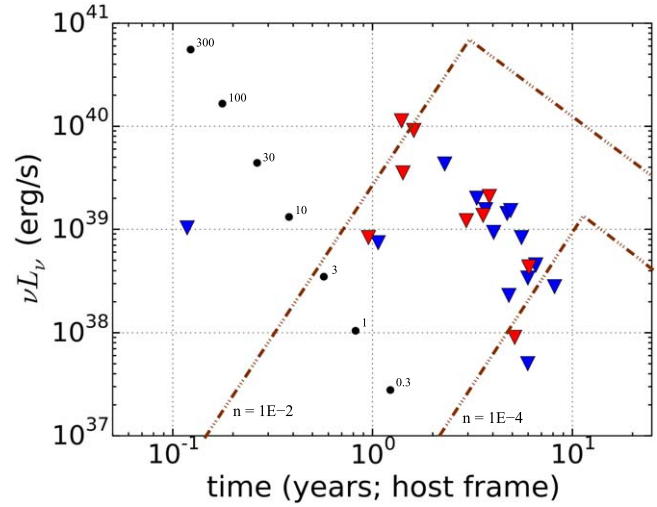

Figure 3. Observational constraints on the 5.5 GHz radio luminosity νL_ν (erg s^{-1}) for 19 short GRBs, mostly years after the corresponding event. In blue are shown our data (Table 5), in red data from Fong et al. (2016b, their Table 1), transformed to an observing frequency of 5.5 GHz. Note that the results for GRB 050724, 070724A, and 130603B are included here twice because these events were independently observed by these authors (at slightly different times after the corresponding burst). In the case of GRB 060502B, the results for two visits are plotted (Table 3). For comparison, we show in dark filled points the predicted peak luminosity and peak time for kilonova radio flares inferred from the numerical merger simulations reported in Radice et al. (2018). Here we used ejecta kinetic energy of 10^{50} and present the results as a function of the circumburst gas density n (in units if cm^{-3}). In addition, two models of magnetar-powered radio flares from Fong et al. (2016b, their Figure 1) are also shown (for $n = 10^{-2}$ and 10^{-4} cm^{-3}; thick dashed–dotted lines). For more details, see the main text.

from short-GRB explosion sites months to years after a burst is not unexpected (see Figure 8 in Chandra & Frail 2012).

Finally, we note that in our time window at 5.5 GHz radio emission from the reverse shock is not expected to be detectable (Resmi & Zhang 2016, their Figure 1).

5.2. Constraints on Late-time Kilonova Radio Flares

According to the picture emerging from GRB 170817A, short bursts originating from compact binary mergers with a NS component should be followed by kilonova light (Lattimer & Schramm 1974; Symbalisty & Schramm 1982; Li & Paczynski 1998). Indeed, at least 5 events from our target list showed evidence for an additional radiation component in their optical/NIR afterglows: GRB 130603B (Berger et al. 2013a; Tanvir et al. 2013), GRB 070809 (Jin et al. 2019), and GRB 050724, 061210, and 150424A (Rossi et al. 2019).

Several authors have pointed out that the interaction of the dynamical mass ejecta with the circumburst medium could produce long-lasting radio emission, a radio flare (Nakar & Piran 2011; Hotokezaka & Piran 2015; Margalit & Piran 2015; Horesh et al. 2016; Hotokezaka et al. 2018; Radice et al. 2018). Moreover, if the merger is followed by the formation of a rapidly spinning magnetar (period $P \sim 1$ ms), a deposition of this energy into the ejecta could result in an even brighter flare (Metzger & Bower 2014; Fong et al. 2016b; Horesh et al. 2016; Kathirgamaraju et al. 2019).

Given the expected peak time, light curve, and potentially high radio luminosity, a kilonova radio flare could be unambiguously identified on times scales of 1–10 yr (e.g., Radice et al. 2018). If detected, radio flares could act as the smoking gun of past kilonova events. However, no such signal has yet been reported.

Figure 3 summarizes the upper limits we can set for a kilonova radio signal for a total of 19 events. These include:

(i) 12 short bursts with known redshift from the sample discussed here (Table 2);
(ii) 6 additional short bursts with known redshift studied by Fong et al. (2016b): GRB 051221A, 080905A, 090510, 090515, 100117A, 101219A;
(iii) the short GRB 071227 (Nicuesa Guelbenzu et al. 2014). Even though in this case the host was detected in the radio band, the emission does not arise from the position of the optical afterglow but from the central bulge of the host ($z = 0.381$). The radio data (dt(host frame) $= 4.038$ yr) then constrain the flux from the GRB explosion site to $F_\nu(5.5\,{\rm GHz}) < 35\,\mu{\rm Jy}$ ($5\sigma_{\rm rms}$), i.e., $\nu L_\nu < 9.3 \times 10^{38}$ erg s^{-1}.

We note that for some events several host-galaxy candidates exist. Analogous to Table 4, in these cases we used the redshift of the cosmologically less distant galaxy. Not included in Figure 3 are those 4 events in our sample where no spectroscopic redshift is known (GRB 090621B, 070729, 101224A, 130515A).

For comparison, in Figure 3 we also plot the peak luminosity νL_ν computed at 5.5 GHz and the peak time emission of the radio flare produced by the interaction of the dynamical ejecta with the surrounding interstellar medium as given by the analytical estimate of Hotokezaka & Piran (2015). The model assumes ejecta kinetic energy $E_{\rm kin} = 10^{50}$ erg and velocities $v_{\rm ej} = 0.3c$ as inferred from numerical relativity simulations Hotokezaka et al. (2018),

Radice et al. (2018). The microphysical parameters are fixed to $\epsilon_B = 0.01$, $\epsilon_e = 0.1$, $p = 2.4$. We also plot a model for a magnetar-powered radio flare as it is discussed by Fong et al. (2016b) and where we have chosen two values for the circumburst gas density ($n = 10^{-2}$, $10^{-4}\,\mathrm{cm}^{-3}$), a rotational energy of the magnetar of $E_{\rm rot} = 10^{53}$ erg and an ejected mass of $M_{\rm ej} = 0.03\,M_\odot$ (adopting $\epsilon_B = 0.1$, $\epsilon_e = 0.1$, $p = 2.4$).

Our negative observational result augments previous unsuccessful searches for late-time radio flares following short GRBs (Metzger & Bower 2014; Fong et al. 2016b; Horesh et al. 2016). Even though most of our data explore a parameter space similar to what was already discussed by these authors, we provide four more events with secure host-galaxy identification and spectroscopic redshift (GRB 061006, 061210A, 100206A, 100816A). GRB 100206A is included in this list, as the radio emission does not arise from a position inside the *Swift*/XRT error circle but from the central bulge of the suspected host (Figure 1). In other words, this is not kilonova emission.

The observations imply that in the time window between about 1 and 10 yr (host frame) kilonova radio flares exceeding a luminosity of $\sim 10^{39}\,\mathrm{erg\,s^{-1}}$ are either rare or do not exist. In principle, a general nondetection of these flares can still be explained within the allowed broad parameter space of the underlying models, including the not well constrained microphysical parameters ϵ_B and ϵ_e and the uncertainties on the circumburst number density n. In any case, the potentially very luminous radio flares predicted by models which rely on magnetar-powered energy deposition into the ejecta were not found in our investigation.

6. Summary and Conclusions

We performed a deep radio-continuum survey of 16 short GRB hosts, with the original goal to search for optically obscured star-forming activity. Only one host was detected (GRB 100206A; $z = 0.407$). Its detection was not surprising, however, as a high radio flux was already expected based on its observed broad-band SED in the optical/IR bands (Perley et al. 2012; Nicuesa Guelbenzu et al. 2014).

Combining our radio data with published data shows that at least five of about 40 short-GRB hosts compiled by Berger (2014) have a relatively high SFR of $>10\,M_\odot\,\mathrm{yr}^{-1}$ (GRB 071227, 100206A, 100816A, 101219A, 120804A).

The present database show that galaxies forming stars at a high rate are not uncommon among the short-GRB host-galaxy population. However, whether this implies a physical link between recent star-forming activity and the formation of short-lived short-GRB progenitors is not clear. At least in the case of GRB 071227 and 100206A, the radio emission which traces the star formation activity does not arise from the GRB explosion site. Furthermore, at least three of these five hosts are characterized by a relatively large stellar mass (GRB 071227, 100206A, 120804A; see Nicuesa Guelbenzu et al. 2014, their Table 1). As noted by several authors (e.g., Leibler & Berger 2010; Fong & Berger 2013; Berger 2014), it could just be the large reservoir of stars which increases the probability of a NS–NS merger to occur (for detailed stellar population synthesis models see, e.g., Tauris et al. 2017; Belczynski et al. 2018).

In conclusion, in the local universe ($z < 0.3$) star-forming short-GRB host galaxies are not forming stars at very high rates. There is no observational evidence for optically obscured star formation. The first extensively star-forming short-GRB hosts appear in the redshift range from $z = 0.3$ to 0.5 (GRB 071229 and 100206A). The data suggest that beyond $z = 0.3$ a non-negligible fraction of short-GRB hosts is forming stars at a high rate.

In addition to our search for optically obscured star formation activity, we used our radio data to derive deep upper limits on the luminosity of the corresponding GRB afterglows and predicted late-time radio flares following short-GRB kilonovae. While the general nondetection of a radio afterglow on timescales of months to years after a short burst is not surprising, our data provide valuable constraints on kilonova magnetar models. By adding 12 more events with redshift information, we substantially increased the available data set for quantifying the luminosities of radio flares in the time frame between 1 and 10 yr (host-frame time) post burst. Their general nondetection places severe constraints on the most extreme kilonova models (e.g., Fong et al. 2016b). The existence of very bright and long-lasting radio flares as predicted by these models is not supported by the data.

To draw more definitive conclusions on the age distribution of the short-GRB progenitor population and the existence or non-existence of radio flares, more and better data are needed. In particular, hosts at low redshifts may act as future "*Rosetta* Stone events"; the host of GRB 170817A at $d \sim 40$ Mpc (Abbott et al. 2017a; Coulter et al. 2017; Kim et al. 2017; Smartt et al. 2017) is the first such promising case in this new sample of LIGO/Virgo-selected events.

S.K. and A.N.G. acknowledge support by the Thüringer Ministerium für Bildung, Wissenschaft und Kultur under FKZ 12010-514 and by grants DFG Kl 766/16-1 and 766/16-3. L.K.H. is grateful for funding from the INAF PRIN-SKA 2017 program 1.05.01.88.04. M.J.M. acknowledges the support of the National Science Centre, Poland through the SONATA BIS grant 2018/30/E/ST9/00208 and the POLONEZ grant 2015/19/P/ST9/04010; this project has received funding from the European Union's Horizon 2020 research and innovation programme under the Marie Skłodowska-Curie grant agreement No. 665778. A.R. acknowledges support from Premiale LBT 2013. S.B. acknowledges support by the EU H2020 under ERC Starting Grant, no. BinGraSp-714626. This paper is based on observations collected with the Australia Telescope Compact Array (ATCA; programme ID C2840, PI: A. Nicuesa Guelbenzu), the NSF's *Karl G. Jansky* Very Large Array (VLA; programme ID 13B-313, 14B-201, 15B-214, PI: A. Nicuesa Guelbenzu), VLT (ESO programme ID 088.D-0657, PI: A. Nicuesa Guelbenzu and programme ID 383.A-0399, PI: S. Klose), as well as GROND at the MPG 2.2 m telescope at ESO La Silla Observatory (PI: J. Greiner), BUSCA at the Calar Alto 2.2 m (PI: J. Gorosabel) and publicly available data obtained from the ESO-VLT, the Gemini and the *Hubble Space Telescope* data archives. The Australia Telescope is funded by the Commonwealth of Australia for operation as a National Facility managed by CSIRO. S.K. and A.N.G. thank Catarina Ubach & Sarah Maddison, Swinburne University, Ivy Wong, Martin Bell, & Mark Wieringa CSIRO Sydney, and Jamie Stevens, CSIRO Narrabri, for very helpful discussions and observing guidance. In particular, Sarah Maddison substantially helped performing remote observations. The National Radio Astronomy Observatory is a facility of the National Science Foundation operated under cooperative agreement by Associated Universities, Inc. S.K. and A.N.G. thank the staff at NRAO (Socorro, NM) for

their hospitality during two visits, in particular Dale Frail, Heidi Medlin, Drew Medlin, and Jürgen Ott. We thank the staff at NRAO for performing the observations. This publication makes use of data products from the *Wide-field Infrared Survey Explorer*, which is a joint project of the University of California, Los Angeles, and the Jet Propulsion Laboratory/California Institute of Technology, funded by the National Aeronautics and Space Administration. This work made use of data supplied by the UK Swift Science Data Centre at the University of Leicester. Part of the funding for GROND (both hardware and personnel) was generously granted by the Leibniz-Prize to G. Hasinger (DFG grant HA 1850/28-1) and by the Thüringer Landessternwarte Tautenburg. We thank the referee for a very careful reading of the manuscript and many valuable suggestions which helped to improve the paper substantially.

Software: MIRIAD (v1.5; Sault et al. 1995), CASA (v5.1.2-4; McMullin et al. 2007).

Appendix
Notes on Individual Targets

General. Enhanced *Swift*/XRT error circle data were taken from http://www.swift.ac.uk/xrt_positions/ (Goad et al. 2007; Evans et al. 2009). In the following, all reported XRT coordinates with their corresponding error radii refer to 2019 January (90% c.l.).

Follow-up observations of short-GRBs in the radio band are summarized in Chandra & Frail (2012) and Fong et al. (2015). The following bursts from our target list have reported radio observations within some days after the event: GRB 050724, 061210A, 070724, 070729, 090612B, 101224A, 130603B, and 150424A. Detected were only the radio afterglows of GRB 050724, 130603B, and 150424A (see Fong et al. 2015, their Table 8).

GRB 050724. The initial pulse of the burst was hard and had a FRED-like profile. It was followed by softer emission; T_{90}(15–350 keV) = 3 ± 1 s (Krimm et al. 2005). Its observed spectral lag is consistent with those of short bursts (Gehrels et al. 2006). The afterglow and its host galaxy are in detail discussed in the literature (Berger et al. 2005; Gorosabel et al. 2006; Prochaska et al. 2006; Malesani et al. 2007; Fong et al. 2011). The optical afterglow was located in the outskirts of a relatively bright galaxy ($R \sim 20$ mag) at a redshift of $z = 0.258$. A global host extinction of $A_v^{\rm host} \sim 0.4$ mag was derived by Gorosabel et al. (2006). The radio afterglow was detected with the VLA 0.6 days after the burst at 8.46 GHz ($F_\nu = 173\ \mu$Jy). It was only seen again one day later at 8.46 GHz ($F_\nu = 465\ \mu$Jy; Berger et al. 2005; Fong et al. 2015).

Several authors have classified the host as an elliptical galaxy (e.g., Berger et al. 2005). Though Malesani et al. (2007) found that it shows a faint outer spiral structure, suggesting that is a disk galaxy with a light-dominating central bulge. This conclusion was strengthened by *HST* images (see Figure 3 in Fong et al. 2011).

Based on optical spectroscopy, the galaxy has a very low star formation rate. Reported upper limits are 0.02 $M_\odot$ yr^{-1} (Berger et al. 2005), 0.05 $M_\odot$ yr^{-1} (Prochaska et al. 2006), and 0.17 $M_\odot$ yr^{-1} (Malesani et al. 2007).

GRB 060502B. The *Swift*/BAT light curve consists of two spikes. According to Sato et al. (2006), T_{90}(15–350 keV) = 90 ± 20 ms, while according to Krimm et al. (2006), D'Avanzo et al. (2014) it is T_{90}(15–350 keV) = 140 ms. No optical afterglow was found. The burst and its suspected host are in detail discussed by Bloom et al. (2007). According to these authors, the most likely host-galaxy candidate is a relatively bright early-type galaxy ($R \sim 18.7$ mag, $z = 0.287$) ∼17.″5 south of the XRT error circle (see their Figure 1). However, publicly available Gemini-N/GMOS images (programme ID GN-2006A-Q-14 PI: B. Schmidt) taken in 2006 May clearly reveal a disk component with at least one spiral arm in both directions. Based on the [O II] emission line, Bloom et al. (2007) calculated a SFR of 0.4–0.8 $M_\odot$ yr^{-1}. Berger et al. (2007) (their Figure 1) pointed out that a much fainter galaxy ($R \sim 25.8$ mag) is located inside the XRT error circle. Its redshift is not known.

GRB 061006. The burst began with an intense double-spike, followed by lower-level persistent emission. Including this radiation component the duration is T_{90}(15–350 keV) = 130 ± 10 s (Krimm et al. 2006). The burst was also seen by the Suzaku Wideband All-sky Monitor (WAM) and T_{90}(50 keV–5 MeV) = 0.42 s (Urata et al. 2006a). The optical afterglow was found with VLT/FORS1 (Malesani et al. 2006a, 2006b). In Gemini-S/GMOS images the host galaxy appears as a faint ($R_C \sim 24.0$ mag) and fuzzy object (see Figure 1 in Berger et al. 2007). Its shows weak emission lines from the [O III] doublet, Hβ, and [O II] at a common redshift of $z = 0.4377 \pm 0.0002$. The [O II] line flux corresponds to a SFR of 0.02 $M_\odot$ yr^{-1} (Berger 2009).

HST observed the field in several occasions between 2006 October and 2007 November using ACS in the NIR (filter F814W; programme ID 10917, PI: D. Fox). The host is an inclined, nearly edge-on spiral galaxy. The optical afterglow was located close to the galactic bulge (see Figure 9 in Fong et al. 2011).

GRB 061201. The burst had a double-peak structure, there is no evidence for extended emission. Its duration was T_{90}(15–350 keV) = 0.8 ± 0.1 s (Markwardt et al. 2006); D'Avanzo et al. (2014) give T_{90}(15–350 keV) = 0.78 s. On VLT/FORS2 images the suspected host is a bulge-dominated galaxy ∼17″ NW from the afterglow (in the following G1; see Figure 5 in Stratta et al. 2007). Long-slit spectroscopy revealed emission lines from [O II] and Hα at a common redshift of $z = 0.111$. Similar results were reported based on *Magellan* observations (Berger 2006a). The SFR based on the Hα flux is 0.14 $M_\odot$ yr^{-1} (Stratta et al. 2007).

The field was observed by *HST* in three different epochs between 2007 and 2013 (programme ID 12502, PI: A. Fruchter). Although the *HST* image goes deeper than the VLT image, at the position of the optical transient there is no evidence for an underlying galaxy. However, inside the 1.″4 XRT error circle lies a faint galaxy (G2) that is not visible on the VLT/FORS2 images. It is located ∼1.″8 southeast of the optical transient ($r \sim 25.5$ mag; see Figure 10 in Fong et al. 2011). There is no redshift information. The position of this galaxy close to the optical transient classifies it as second host-galaxy candidate.

GRB 061210. The *Swift*/BAT light curve shows a hard FRED-like spike, followed by extended, soft emission; T_{90}(15–350 keV) is 85 ± 5 s (Palmer et al. 2006). The burst was also seen by Suzaku/WAM and T_{90}(50 keV–5 MeV) = 0.047 s (Urata et al. 2006b).

No optical afterglow was found. A host-galaxy candidate was first identified by Berger (2006b), its redshift is 0.41 (Cenko et al. 2006; Berger et al. 2007). On archived Gemini-N/GMOS images the host appears as a bulge-dominated galaxy (see Figure 1 in Berger et al. 2007). According to Berger (2014), its SFR is 1.2 $M_\odot$ yr^{-1}.

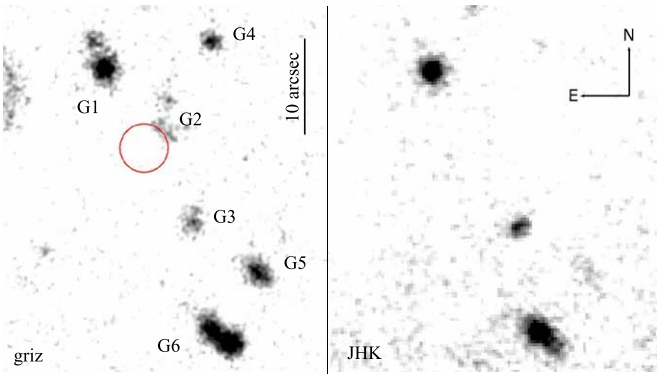

Figure 4. GROND combined $g'r'i'z'$ and JHK_s-band image of the field of GRB 070729. Also shown is the *Swift*/XRT error circle ($r = 2\farcs5$). Galaxies close to the error circle are labeled. No radio source has been found in this field. (The extended faint structure seen in the $g'r'i'z'$-band image close to the upper left corner is a ghost image from a bright star.)

GRB 070724A. In the *Swift*/BAT energy band the burst showed a single spike. According to Parsons et al. (2007), T_{90}(15–350 keV) was 0.4 ± 0.04 s, while according to D'Avanzo et al. (2014) it was 0.43 s. The discovery of the optical/NIR afterglow was reported by Berger et al. (2009a) (see their Figure 1). These authors also studied the host galaxy which lies at a redshift of $z = 0.457$ (see also Kocevski et al. 2010, their Figure 3). The optical/NIR afterglow was affected by about 2 mag host-galaxy visual extinction along the line of sight (Berger et al. 2009a), indicating that this is a dust-rich host. Optical spectra revealed a global SFR between about 1 and 100 $M_\odot$ yr^{-1}; internal host-galaxy extinction made a more robust measurement difficult (Kocevski et al. 2010). According to Berger (2014), the SFR is 2.5 $M_\odot$ yr^{-1}.

GRB 070729. The *Swift*/BAT light curve showed two overlapping peaks. According to Sato et al. (2007), T_{90}(15–350 keV) $= 0.9 \pm 0.1$ s, while D'Avanzo et al. (2014) measure T_{90}(15–350 keV) $= 0.99$ s. Follow-up observations did not reveal an afterglow, either in the optical (for GROND see Küpcü Yoldaş et al. 2008) or in the radio band (Chandra & Frail 2007). At the western border of the enhanced XRT error circle lie two (or three) faint objects (G2; Küpcü Yoldaş et al. 2008). Several additional brighter galaxies lie some arcsec away (G1, G3, and G4–G6; Figure 4).

The field was also studied by Leibler & Berger (2010). Based on their broad-band photometry these authors derived a photometric redshift for G3 of $z = 0.8 \pm 0.1$. No spectroscopic redshifts are known. The GROND data suggest that G1, G3, and G6 are dusty star-forming galaxies, probably at the same redshift. G1 and G6 have been detected by the *WISE* satellite (G1 is listed in Table 1). G1 and G3 are very red objects ($(r' - K_s)_{\rm AB} \sim 3$ mag). We consider G1–G3 as host-galaxy candidates. None of these labeled galaxies (G1–G6) has been detected in our ATCA observing run.

GRB 070809. The *Swift*/BAT light curve shows a single peak. According to Krimm et al. (2007), T_{90}(15–350 keV) $= 1.3 \pm 0.1$ s, while according to D'Avanzo et al. (2014), it is T_{90}(15–350 keV) $= 1.28$ s. The recent possible detection of kilonova light in the GRB afterglow confirms the short-burst nature of this event (Jin et al. 2019).

Observations with the Keck telescope did not reveal an underlying host galaxy either at the position of the optical afterglow or within the $3\farcs6$ XRT error circle (Perley et al. 2008). The galaxy nearest to the optical afterglow is an edge-on spiral $6''$ northwest (named "S2" in Figure 2 in Berger 2010). At a redshift of $z = 0.2187$ this galaxy lies at a projected distance of $\sim$22 kpc from the optical afterglow. Its flux in the [O II] line corresponds to an optical SFR of 0.15 $M_\odot$ yr^{-1}. A second galaxy (named "S3" in Berger 2010) lies $6''$ west from the optical transient. It is an E0 elliptical at a redshift of $z = 0.473$, with no evidence for star formation.

The field was also observed by *HST* in 2009 August and 2010 May with two different filters (F606W/F160W; programme ID 12502, PI: A. Fruchter). At the position of the optical afterglow there is no underlying host galaxy either at the optical (>28.1 mag) or in the NIR ($H > 26.2$ mag; Fong & Berger 2013). The *HST* observations revealed the presence of a faint background galaxy inside the XRT error circle (named "S1" in Berger 2010). Its redshift is not known.

No radio flux was detected either from the three designated galaxies or from the position of the optical transient.

GRB 080123. In the *Swift*/BAT energy window the burst showed a FRED-like profile, followed by soft, extended emission. T_{90}(15–350 keV) was 115 ± 30 s (Tueller et al. 2008). This was refinded to 115.18 s by D'Avanzo et al. (2014). Suzaku/WAM also detected the burst with a duration T_{90}(50 keV–5 MeV) of about 0.40 s (Uehara et al. 2008). No optical afterglow was found. VLT/FORS2 R_C-band and ISAAC K_s-band imaging of the field was obtained in 2009 May (ESO programme ID 383.A-0399; PI: S. Klose). Inside the $1\farcs7$ XRT error circle, the VLT images do not reveal any source down to $R_C = 27.0$ mag and $K_s = 23.3$ mag. An optical faint source (G2) lies at the border of the XRT error circle, another source around $3''$ away (G3; Figure 5). G2 and G3 are very faint in the R_c band ($\sim$25.5 mag) and not detected down to $K_s = 23.3$ mag.

The most prominent object in the field is a galaxy (G1, $z = 0.496$; $R_C = 19.6$ mag) $\sim 8''$ northeast of the center of the XRT error circle (Leibler & Berger 2010). It is the most likely host-galaxy candidate. The FORS2 R_C-band image reveals that this is an inclined, barred spiral with two symmetric spiral arms.

Long-slit spectroscopy of G1 was obtained with VLT/FORS2 in 2011 October and November using the *GRIS 600B* and *GRIS 600RI* grism (PI: A. Nicuesa Guelbenzu, ESO programme ID 088.D-0657), covering the wavelength range from 3300 Å to 8450 Å. The spectral slit was oriented along the major axis of the galaxy G1. The spectrum shows emission lines of Hβ, Hγ, and [O III] at a common redshift of $z = 0.496$, in agreement with what was reported by Leibler & Berger (2010). The blue spectrum obtained with the *GRIS 600B* is of less quality; no emission or absorption lines could be identified. The (not extinction-corrected) SFR based on the measured Hβ line flux in the FORS2 spectrum is 0.7 $M_\odot$ yr^{-1}.

No redshift could be derived for G2. Although during the FORS2 observations the spectral slit was covering this galaxy, no trace of this object could be identified. None of these galaxies was detected in our radio observations.

GRB 090621B. The bursts showed a single peak, in the *Swift*/BAT energy band T_{90}(15–350 keV) $= 0.14 \pm 0.04$ s (Krimm et al. 2009). The burst was also detected by *Fermi*/GBM and T_{90}(8–1000 keV) $= 0.128$ s (Goldstein & Burgess 2009). The X-ray afterglow was rather faint (Beardmore et al. 2009), no optical afterglow was found. A single, faint object inside the XRT error circle ($I \sim 22.9$ mag; Cenko et al. 2009; Galeev et al. 2009;

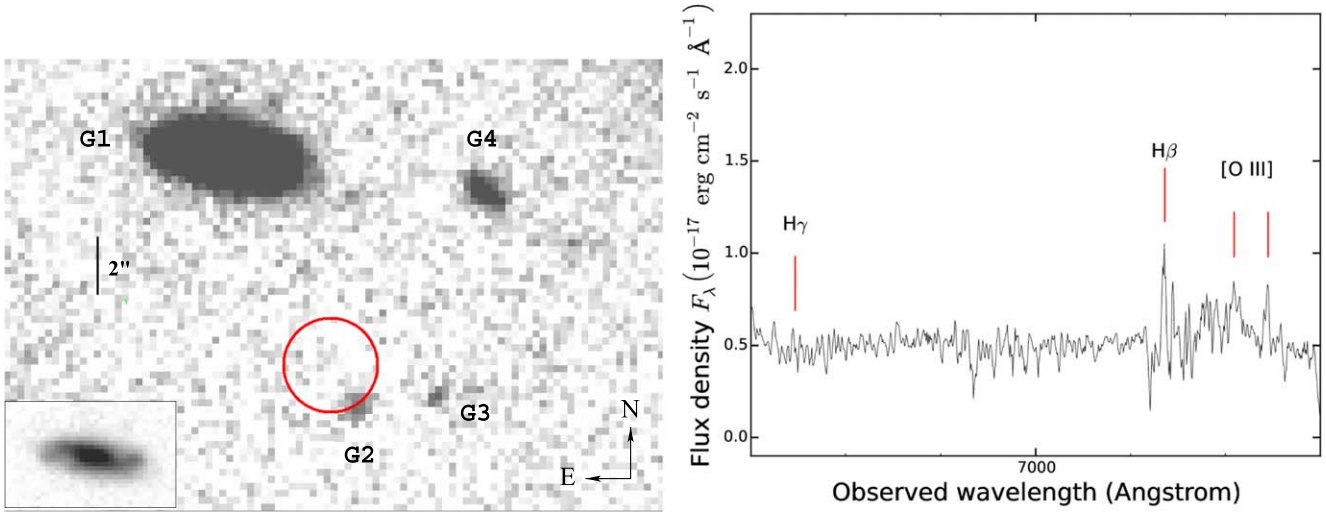

Figure 5. Left panel: VLT/FORS2 R_C-band image of the field of GRB 080123. In red it is shown the $r = 1\farcs7$ XRT error circle. Among the four galaxies close to the error circle G1 is the most likely host-galaxy candidate (Leibler & Berger 2010). The inset shows the spiral structure of G1 as it appears after changing the contrast parameters in the VLT image. Right panel: VLT/FORS2 spectrum of G1. It shows emission from the [O III] doublet, Hβ and Hγ at a common redshift of $z = 0.496$.

Levan et al. 2009) turned out to be an M star (Berger et al. 2009b). No host-galaxy candidate has been reported so far.

Our VLA radio data reveal a radio source (F_ν(5.5 GHz) = 58 ± 6 μJy), 45″ south of the XRT error circle), at coordinates R.A., decl. (J2000) = 20:53:53.70, 69:00:55.7. A comparison with our optical observations of the field in 2012 July using the Calar Alto 2.2 m telescope (observer: J. Gorosabel) shows at this position a galaxy (Figure 6). Its morphology cannot be determined with certainty. On our 2.2 m/BUSCA *i*-band image its size is about $4\farcs5 \times 5\farcs2$, with the long axis oriented in northwest–southeast direction. Its redshift is not known. The GRB progenitor exploded at a projected distance of ∼280/340/360 kpc (for $z = 0.5/0.8/1.0$) from this object.

GRB 100206A. In the *Swift*/BAT energy window the burst showed a single spike, T_{90}(15–350 keV) = 0.12 ± 0.03 s (Sakamoto et al. 2010). Also *Fermi*/GBM detected the burst; T_{90}(8–1000 keV) = 0.13 ± 0.05 s (von Kienlin 2010). No optical afterglow was found. Perley et al. (2012) performed a comprehensive study of the burst and its host and concluded that this is a dusty, infrared bright galaxy ($L_{\rm IR} \sim 4 \times 10^{11}\,L_\odot$) at $z = 0.4068$ with a global host extinction of $A_{\rm V}^{\rm host} = 2$ mag and a star formation rate of about 30 $M_\odot$ yr^{-1}. According to its position in the *WISE* color–color diagram (Wright et al. 2010), this is a starburst galaxy (Section 2). Perley et al. (2012) have pointed out that close to this galaxy (in the following G1) lies a ∼4 mag fainter galaxy (in the following G2). Its redshift is 0.803. Several arguments suggest that G1 is the primary host galaxy candidate while G2 is a background galaxy (Figure 1).[19]

GRB 100816A. The burst was detected by *Swift*/BAT and *Fermi*/GBM. In the BAT energy window it consisted of a single spike with a duration T_{90}(15–350 keV) = 2.9 ± 0.6 s (Markwardt et al. 2010a; D'Avanzo et al. 2014), while for GBM T_{90}(50–300 keV) ∼ 2 s (Fitzpatrick 2010). The nature of this burst is debated. With its duration the burst lies intermediate between long and short-population bursts. Its spectrum was hard, characteristic for a short burst, but with a low peak energy (Fitzpatrick 2010). Its observed spectral lag in the *Swift*/BAT energy window is consistent with zero, though the errors are relatively large (Norris et al. 2010; Bernardini et al. 2015). Other burst and afterglow properties move the burst closer to the long-burst population (D'Avanzo et al. 2014).

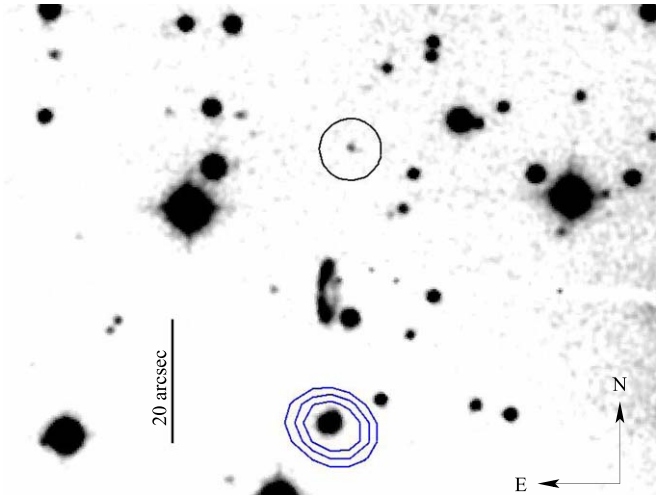

Figure 6. *i*-band image of the field of GRB 090621B taken with BUSCA at the Calar Alto 2.2 m telescope in 2012 July. According to Berger et al. (2009b), the faint source inside the XRT error circle (in black; radius $r = 3\farcs3$) is an M star. Overlaid are the VLA radio contours in the field at 5.5 GHz (in blue; corresponding to 3, 4, and 5 μJy beam^{-1}). A bright radio source lies south of the XRT error circle. Note that the elongated object between the XRT error circle and the radio source is an artifact in the image.

Its optical afterglow was found by *Swift*/UVOT (Oates et al. 2010). It was well offset from its host (Im et al. 2010); its redshift is $z = 0.8049$ (Gorosabel et al. 2010; Tanvir et al. 2010). No late-time supernova signal was detected down to 0.1 the peak luminosity of SN 1998bw (Tunnicliffe & Levan 2012), supporting the interpretation that GRB 100816A belongs to the short-burst population.

The afterglow was situated in the northern region of its host, about $1\farcs3$ away from the host galaxy center (for the given redshift this corresponds to about 10 kpc projected distance). In

[19] Note that the revised XRT coordinates, R.A., decl. (J2000) = 03:08:39.00, 13:09:24.8 (radius $3\farcs2$; as of 2019 January) are slightly different from the XRT coordinates used in Perley et al. (2012).

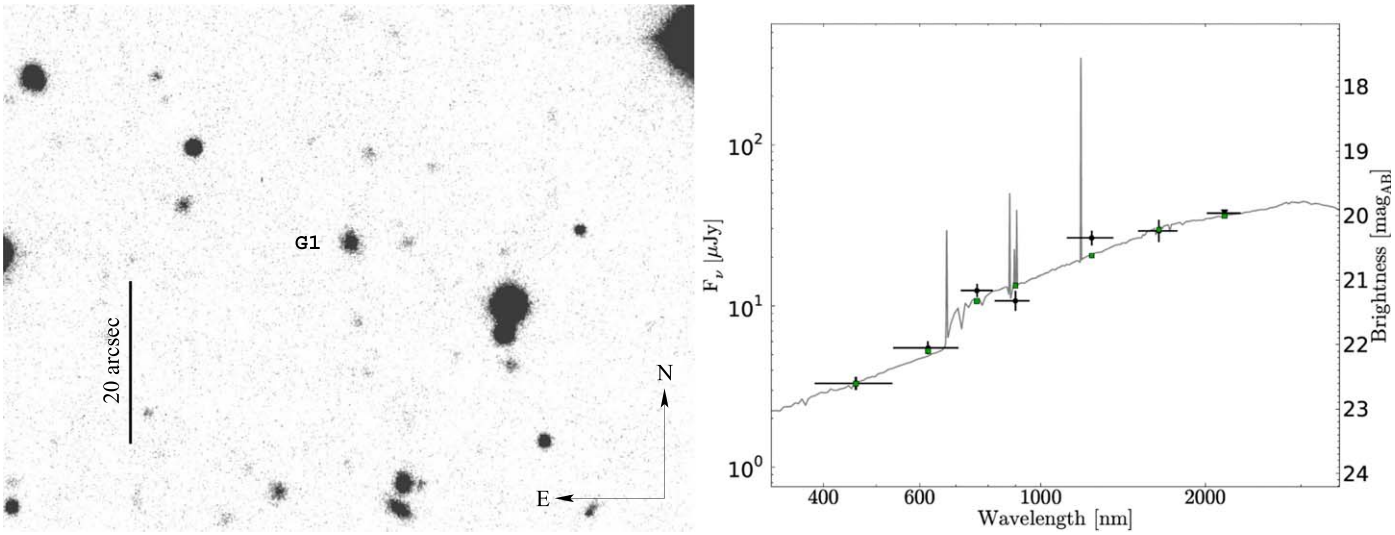

Figure 7. Left: GROND $g'r'i'z'$ (white)-band image of the host galaxy of GRB 100816A (G1) taken on 2010 August 18. There is no OT detected anymore. There is no radio source in this field. Right: Broad-band ($g'r'i'z'JHK_s$) SED of G1 based on GROND multi-color data and the best fit using the `Le Phare` package (corrected for a Galactic reddening along the line of sight of $E(B-V) = 0.096$ mag; Schlegel et al. 1998).

the combined GROND white-band the galaxy appears morphologically disturbed in northeast direction. It is a bulge-dominated galaxy seen nearly face-on (G1; Figure 7). The host galaxy of GRB 100816A was also detected by *WISE* in the *W1* and *W2* bands, but not in *W3* and *W4*.

Based on VLT/X-Shooter spectra, Krühler et al. (2015) find that the host is a dusty galaxy ($E(B-V)_{\rm host} = 1.32$ (+0.24, −0.22) mag) with an SFR of $58^{+51}_{-26}\ M_\odot\ {\rm yr}^{-1}$ and a metallicity of $12 + \log({\rm O/H}) = 8.75^{+0.16}_{-0.18}$. The observed mass–metallicity relation for galaxies at $z \sim 0.7$ (Mannucci et al. 2009; Mapelli et al. 2018) then implies a mass in stars of about log $M/M_\odot = 9.2 - 10.2$. The galaxy was also studied by Pérez-Ramírez et al. (2013) using the Spanish 10 m Gran Telescopio CANARIAS (GTC) and the telescopes at Calar Alto. These authors found that the SED is best fit by a starburst galaxy. According to our GROND photometry, this is a luminous ($M_B = -21.7$ mag), dusty ($E(B\text{-}V)_{\rm host} = 0.4$ mag), massive (log $M/M_\odot = 10.4 \pm 0.4$) galaxy with an SFR between 40 and 400 $M_\odot\ {\rm yr}^{-1}$ (Figure 7).

GRB 101224A. In the *Swift*/BAT band the burst showed a multipeak structure, T_{90}(15–350 keV) = 0.2 ± 0.01 s (Markwardt et al. 2010b; D'Avanzo et al. 2014). It was followed by a rather faint X-ray afterglow which was rapidly fading (Pagani & Krimm 2010). No optical afterglow was detected (Kuroda et al. 2010; Landsman & Krimm 2010), no radio afterglow was found (Zauderer et al. 2011). A faint object inside the XRT error circle was discovered by Nugent & Bloom (2010). It was later confirmed by Xu et al. (2010) and found to be a galaxy. Its morphology cannot be determined on our images (Figure 8).

Our VLA observations reveal a radio source (F_ν(5.5 GHz) = 235 ± 7 μJy) 35″ southwest of the XRT error circle at coordinates R.A., decl. (J2000) = 19:03:39.90, 45:42:20.5 (Figure 8). Its redshift is not known.

GRB 130515A. The burst was seen by several instruments: (i) *Swift*/BAT: T_{90}(15–150 keV) = 0.29 ± 0.06 s (Barthelmy et al. 2013a; D'Avanzo et al. 2014), (ii) Suzaku/WAM: T_{90}(50 keV–5 MeV) = 0.25 s (Iwakiri et al. 2013), (iii) *Fermi*/GBM: T_{90}(50–300 keV) = 0.26 s (Jenke 2013). No optical afterglow was found. Using archived VLT/FORS2 R_C-band data (ESO programme ID 091.D-0558; PI: A. Levan; Levan & Tanvir 2013), the galaxy closest to the 2.″2 XRT error circle lies ∼8.″5 southwest of the XRT position at coordinates R.A., decl. (J2000) = 18:53:44.98, −54:16:50.9 (Figure 9). Its spectroscopic redshift is not known.

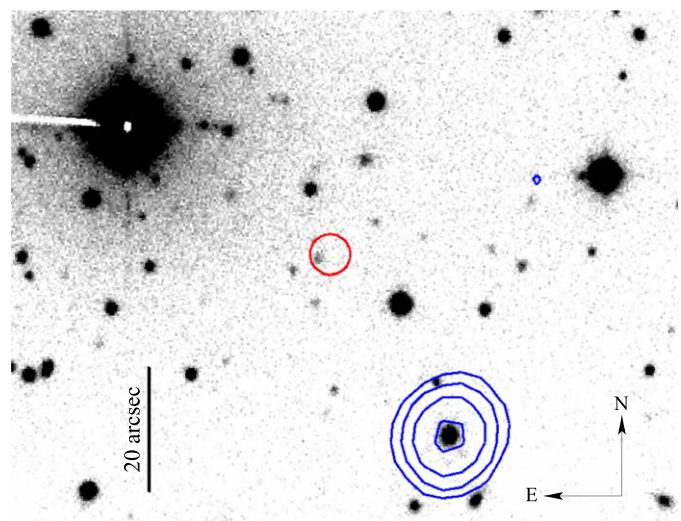

Figure 8. Calar Alto 2.2 m/BUSCA *i*-band image of the field of GRB 101224A, taken in 2012 June (observer: J. Gorosabel). In red is shown the $r = 3.''2$ XRT error circle. Inside the error circle lies a faint galaxy ($R \sim 21.5$ mag; Nugent & Bloom 2010; Xu et al. 2010). In blue is shown a contour plot of our VLA 5.5 GHz observations. A bright radio source lies southwest of the center of the XRT error circle. Contour lines correspond to 2, 5, 10, 20 μJy beam^{-1}.

GRB 130603B: The burst was detected by *Swift*/BAT. It showed a single FRED-like spike, T_{90}(15–350 keV) = 0.18 ± 0.02 s (Barthelmy et al. 2013b; D'Avanzo et al. 2014). Its observed spectral lag in the *Swift*/BAT energy window was $-3.44^{7.27}_{5.58}$ ms, consistent with zero (Bernardini et al. 2015). The X-ray/optical afterglow and the host galaxy has been studied in detail by several groups (Cucchiara et al. 2013; de Ugarte Postigo et al. 2014; Fong et al. 2014). These authors found that the afterglow was located in a star-forming galaxy at $z = 0.3565$. The galaxy is very dusty. The line-of-sight extinction to the optical afterglow is about A_V(host) = 0.9 mag, while the

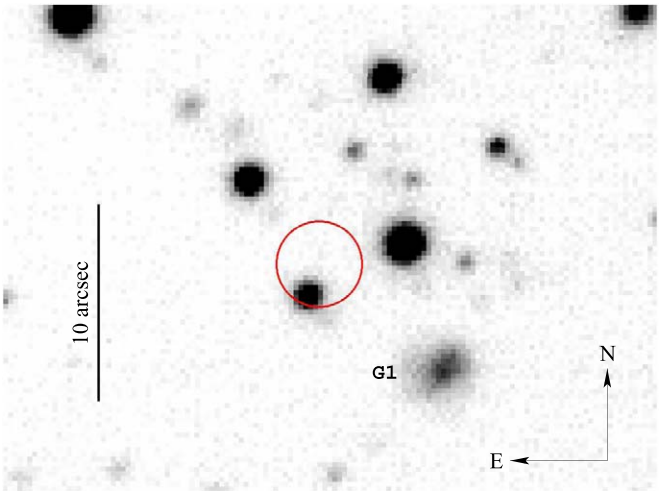

Figure 9. VLT/FORS2 R_C-band image of the field of GRB 130515A (ESO programme ID 091.D-0558; PI: A. Levan). The suspected host galaxy G1 lies $\sim 8\farcs5$ southwest of the center of the XRT error circle (radius $2\farcs2$). There is no radio source in this field.

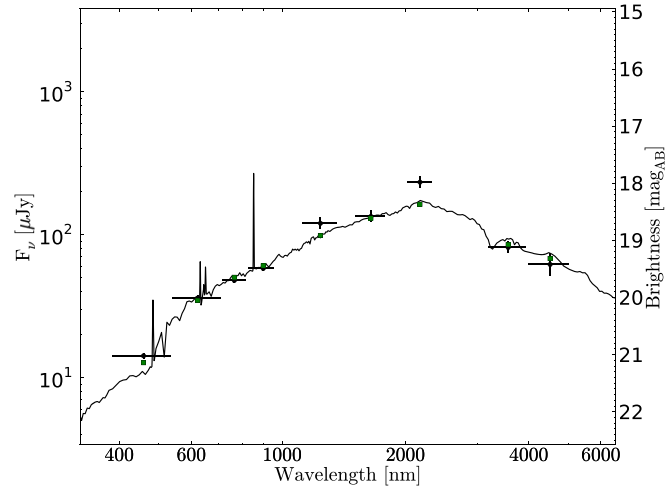

Figure 10. GRB 150424A: `Le Phare` best fit of the broad-band SED of the suspected host galaxy G1 based on GROND $g'r'i'z'JHK_s$-band data as well as the publicly available *WISE* satellite (*W1, W2* filter) data (corrected for a Galactic reddening along the line of sight of $E(B-V) = 0.06$ mag; Schlegel et al. 1998).

global visual extinction of this galaxy is about 1.3 mag. Its extinction-corrected SFR is about 2–5 $M_\odot\,\mathrm{yr}^{-1}$.

The radio afterglow was detected with the VLA 0.37 days after the burst at 4.9 GHz ($F_\nu = 125\,\mu$Jy) and 6.7 GHz ($F_\nu = 119\,\mu$Jy). It was only seen again the following day at 6.7 GHz ($F_\nu = 65\,\mu$Jy; Fong et al. 2014, 2015).

Our nondetection of this galaxy at 5.5 GHz is in agreement with the predicted radio flux of the host in model "MS5" discussed by Contini (2018, her Figure 4). According to this model at 5.5 GHz one expects $\log \nu F_\nu \sim -18.2$, while we measure $\log \nu F_\nu < -17.8$ (in units of erg cm^{-2} s^{-1}).

GRB 150424A. In the *Swift*/BAT energy window the burst showed a bright multi-peaked episode followed by extended emission, T_{90}(15–350 keV) $= 91 \pm 22$ s (Barthelmy et al. 2015). The burst triggered also Konus-*Wind*. Here it showed a multipeak structure with a total duration of about 0.4 s (Golenetskii et al. 2015). The optical/X-ray afterglow parameters and its physical implications are in detail discussed in Kaplan et al. (2015), Knust et al. (2017), and Jin et al. (2018). The radio afterglow was discovered with VLA about 18 hr after the burst (F_ν (9.8 GHz) $\sim$31 μJy; Fong 2015).

Follow-up observations performed with the Spanish GTC 10 m telescope (programme ID GTC72-15A; PI: A. Castro-Tirado) revealed the presence of a spiral galaxy $2''$ southwest to the optical transient (G1; see Figure 1 in Jin et al. 2018) and Figure 2 in Knust et al. (2017). Castro-Tirado et al. (2015) reported a redshift of $z = 0.3$ for G1. In a reanalysis of this spectrum we found emission from Hα, [S II] as well as the [N II] doublet at a common redshift of $z = 0.2981 \pm 0.0001$. The flux in the Hα line is more prominent in the western part than in the eastern part of the galaxy (28×10^{-17} erg s^{-1} cm^{-2} versus 13×10^{-17} erg s^{-1} cm^{-2}). In total its flux corresponds to a SFR of 0.15 $M_\odot\,\mathrm{yr}^{-1}$. Since the spectral slit covered only one-third of the apparent width of the galaxy a more realistic estimate of the optical SFR is 0.5 $M_\odot\,\mathrm{yr}^{-1}$.

Figure 10 shows the broad-band SED of G1. Fixing the redshift to $z = 0.3$, `Le Phare` finds that this is a star-forming galaxy (SFR $\sim$7 $M_\odot\,\mathrm{yr}^{-1}$) with an internal reddening of $E(B-V)_{\mathrm{host}} = 0.25$ mag. Its mass in stars is about $10^{10}\,M_\odot$.

Follow-up observations with *HST* revealed the presence of a faint object underlying the position of the optical afterglow (Tanvir et al. 2015). According to these authors this is a faint galaxy at a redshift $z > 0.7$. This is the second host-galaxy candidate (G2).

The VLA detected the radio afterglow 18 hr after the burst at 9.8 GHz as a faint source ($F_\nu = 31\,\mu$Jy) It was not detected anymore 4.8 and 7.9 days after the burst (Fong 2015).

ATCA observations of the field were performed in 2015 June and October, $dt_1 = 0.15$ and $dt_2 = 0.50$ yr after the burst. Unfortunately, during the October run the source position on the sky resulted in a very elongated synthesized beam; we could not reduce these data completely, the MIRIAD/restore command failed. This problem did not occur with the combined ATCA data set. Table 3 lists the beam size and the 1 σ_{rms} error for the combined data set.

The problem with the October run did not affect a setting of constraints on the SFR (none of both galaxies was detected). However, the predicted flux of a kilonova radio flare can be rapidly evolving with time; it can be very different for two different times dt_1 and dt_2 if $dt_2/dt_1 \sim 3$ (see Fong et al. 2016b, their Equation (3) and Figure 1). Therefore, in Figure 3 we plot only the constraint on νL_ν for the first ATCA observing run (for a robust parameter of 0.5 the size of the synthesized beam was $30\farcs4 \times 1\farcs8$ and $1\sigma_{\mathrm{rms}} = 13.5\,\mu$Jy beam^{-1}).

ORCID iDs

L. K. Hunt https://orcid.org/0000-0001-9162-2371
D. H. Hartmann https://orcid.org/0000-0002-8028-0991
J. Greiner https://orcid.org/0000-0002-9875-426X
A. Rossi https://orcid.org/0000-0002-8860-6538
S. Bernuzzi https://orcid.org/0000-0002-2334-0935

References

Abbott, B. P., Abbott, R., Abbott, T. D., et al. 2017a, ApJL, 848, L12
Abbott, B. P., Abbott, R., Abbott, T. D., et al. 2017b, ApJL, 848, L13
Arnouts, S., Cristiani, S., Moscardini, L., et al. 1999, MNRAS, 310, 540
Arnouts, S., Le Floc'h, E., Chevallard, J., et al. 2013, A&A, 558, A67

Barthelmy, S. D., Baumgartner, W. H., Beardmore, A. P., et al. 2015, GCN, 17761, 1
Barthelmy, S. D., Baumgartner, W. H., Cummings, J. R., et al. 2013a, GCN, 14658, 1
Barthelmy, S. D., Baumgartner, W. H., Cummings, J. R., et al. 2013b, GCN, 14741, 1
Beardmore, A. P., Page, K. L., & Curran, P. A. 2009, GCN, 9550, 1
Belczynski, K., Bulik, T., Olejak, A., et al. 2018, arXiv:1812.10065
Belczynski, K., Perna, R., Bulik, T., et al. 2006, ApJ, 648, 1110
Belczynski, K., Stanek, K. Z., & Fryer, C. L. 2007, arXiv:0712.3309
Berger, E. 2006a, GCN, 5952, 1
Berger, E. 2006b, GCN, 5922, 1
Berger, E. 2009, ApJ, 690, 231
Berger, E. 2010, ApJ, 722, 1946
Berger, E. 2014, ARA&A, 52, 43
Berger, E., Cenko, S. B., Fox, D. B., & Cucchiara, A. 2009a, ApJ, 704, 877
Berger, E., Cowie, L. L., Kulkarni, S. R., et al. 2003, ApJ, 588, 99
Berger, E., Cucchiara, A., Fox, D. B., & Levan, A. J. 2009b, GCN, 9559, 1
Berger, E., Fong, W., & Chornock, R. 2013a, ApJL, 774, L23
Berger, E., Fox, D. B., Price, P. A., et al. 2007, ApJ, 664, 1000
Berger, E., Price, P. A., Cenko, S. B., et al. 2005, Natur, 438, 988
Berger, E., Zauderer, B. A., Levan, A., et al. 2013b, ApJ, 765, 121
Bernardini, M. G., Ghirlanda, G., Campana, S., et al. 2015, MNRAS, 446, 1129
Bloom, J. S., Kulkarni, S. R., & Djorgovski, S. G. 2002, AJ, 123, 1111
Bloom, J. S., Perley, D. A., Chen, H.-W., et al. 2007, ApJ, 654, 878
Briggs, D. S. 1995, BAAS, 27, 1444
Bromberg, O., Nakar, E., Piran, T., & Sari, R. 2013, ApJ, 764, 179
Burgay, M., D'Amico, N., Possenti, A., et al. 2003, Natur, 426, 531
Cano, Z. 2016, LPICo, 1962, 4116
Caputi, K. I., Dole, H., Lagache, G., et al. 2006, A&A, 454, 143
Casey, C. M., Narayanan, D., & Cooray, A. 2014, PhR, 541, 45
Castro Cerón, J. M., Michałowski, M. J., Hjorth, J., et al. 2006, ApJL, 653, L85
Castro Cerón, J. M., Michałowski, M. J., Hjorth, J., et al. 2010, ApJ, 721, 1919
Castro-Tirado, A. J., Sanchez-Ramirez, R., Lombardi, G., & Rivero, M. A. 2015, GCN, 17758, 1
Cenko, S. B., Kasliwal, M., Cameron, P. B., Kulkarni, S. R., & Fox, D. B. 2006, GCN, 5946, 1
Cenko, S. B., Levan, A. J., Kasliwal, M. M., & Kulkarni, S. R. 2009, GCN, 9557, 1
Chandra, P., & Frail, D. A. 2007, GCN, 6742, 1
Chandra, P., & Frail, D. A. 2012, ApJ, 746, 156
Chornock, R., & Berger, E. 2011, GCN, 11518, 1
Chrimes, A. A., Stanway, E. R., Levan, A. J., et al. 2018, MNRAS, 478, 2
Christensen, L., Hjorth, J., & Gorosabel, J. 2004, A&A, 425, 913
Contini, M. 2018, A&A, 620, A37
Coulter, D. A., Foley, R. J., Kilpatrick, C. D., et al. 2017, Sci, 358, 1556
Cucchiara, A., Prochaska, J. X., Perley, D., et al. 2013, ApJ, 777, 94
D'Avanzo, P., Malesani, D., Covino, S., et al. 2009, A&A, 498, 711
D'Avanzo, P., Salvaterra, R., Bernardini, M. G., et al. 2014, MNRAS, 442, 2342
de Ugarte Postigo, A., Thöne, C. C., Rowlinson, A., et al. 2014, A&A, 563, A62
Evans, P. A., Beardmore, A. P., Page, K. L., et al. 2009, MNRAS, 397, 1177
Fan, X. L., Yin, J., & Matteucci, F. 2010, A&A, 521, A73
Fitzpatrick, G. 2010, GCN, 11124, 1
Fong, W. 2015, GCN, 17804, 1
Fong, W., & Berger, E. 2013, ApJ, 776, 18
Fong, W., Berger, E., Chornock, R., et al. 2011, ApJ, 730, 26
Fong, W., Berger, E., Chornock, R., et al. 2013, ApJ, 769, 56
Fong, W., Berger, E., & Fox, D. B. 2010, ApJ, 708, 9
Fong, W., Berger, E., Margutti, R., & Zauderer, B. A. 2015, ApJ, 815, 102
Fong, W., Berger, E., Metzger, B. D., et al. 2014, ApJ, 780, 118
Fong, W., & Chornock, R. 2016, GCN, 20168, 1
Fong, W., Margutti, R., Chornock, R., et al. 2016a, ApJ, 833, 151
Fong, W., Metzger, B. D., Berger, E., & Özel, F. 2016b, ApJ, 831, 141
Fruchter, A. S., Levan, A. J., Strolger, L., et al. 2006, Natur, 441, 463
Galeev, A., Bikmaev, I., Sakhibullin, N., et al. 2009, GCN, 9549, 1
Gehrels, N., Norris, J. P., Barthelmy, S. D., et al. 2006, Natur, 444, 1044
Giacomazzo, B., Perna, R., Rezzolla, L., Troja, E., & Lazzati, D. 2013, ApJL, 762, L18
Gioia, I. M., Gregorini, L., & Klein, U. 1982, A&A, 116, 164
Goad, M. R., Tyler, L. G., Beardmore, A. P., et al. 2007, A&A, 476, 1401
Goldstein, A., & Burgess, J. M. 2009, GCN, 9562, 1
Golenetskii, S., Aptekar, R., Frederiks, D., et al. 2015, GCN, 17752, 1
Gorosabel, J., Castro-Tirado, A. J., Guziy, S., et al. 2006, A&A, 450, 87
Gorosabel, J., Castro-Tirado, A. J., Tanvir, N., et al. 2010, GCN, 11125, 1
Greiner, J., Bornemann, W., Clemens, C., et al. 2007, Msngr, 130, 12
Greiner, J., Bornemann, W., Clemens, C., et al. 2008, PASP, 120, 405
Greiner, J., Michałowski, M. J., Klose, S., et al. 2016, A&A, 593, A17
Greis, S. M. L., Stanway, E. R., Levan, A. J., Davies, L. J. M., & Eldridge, J. J. 2017, MNRAS, 470, 489
Hatsukade, B., Hashimoto, T., Ohta, K., et al. 2012, ApJ, 748, 108
Hjorth, J., & Bloom, J. S. 2012, in The Gamma-Ray Burst—Supernova Connection, ed. C. Kouveliotou, R. A. M. J. Wijers, & S. E. Woosley (Cambridge: Cambridge Univ. Press), 169
Horesh, A., Hotokezaka, K., Piran, T., Nakar, E., & Hancock, P. 2016, ApJL, 819, L22
Hotokezaka, K., Kiuchi, K., Shibata, M., Nakar, E., & Piran, T. 2018, ApJ, 867, 95
Hotokezaka, K., & Piran, T. 2015, MNRAS, 450, 1430
Hunt, L. K., Palazzi, E., Rossi, A., et al. 2011, ApJL, 736, L36
Iglesias-Páramo, J., Buat, V., Hernández-Fernández, J., et al. 2007, ApJ, 670, 279
Ilbert, O., Arnouts, S., McCracken, H. J., et al. 2006, A&A, 457, 841
Im, M., Park, W.-K., Pak, S., et al. 2010, GCN, 11108, 1
Iwakiri, W., Tashiro, M., Terada, Y., et al. 2013, GCN, 14688, 1
Jenke, P. 2013, GCN, 14663, 1
Jin, Z.-P., Covino, S., Liao, N.-H., et al. 2019, NatAs, in press
Jin, Z.-P., Li, X., Wang, H., et al. 2018, ApJ, 857, 128
Kann, D. A., Klose, S., Zhang, B., et al. 2011, ApJ, 734, 96
Kaplan, D. L., Rowlinson, A., Bannister, K. W., et al. 2015, ApJL, 814, L25
Kasen, D., Metzger, B., Barnes, J., Quataert, E., & Ramirez-Ruiz, E. 2017, Natur, 551, 80
Kathirgamaraju, A., Giannios, D., & Beniamini, P. 2019, MNRAS, 487, 3914
Kennicutt, R. C., Jr. 1998, ARA&A, 36, 189
Kim, S., Schulze, S., Resmi, L., et al. 2017, ApJL, 850, L21
Klein, U., Lisenfeld, U., & Verley, S. 2018, A&A, 611, A55
Knust, F., Greiner, J., van Eerten, H. J., et al. 2017, A&A, 607, A84
Kocevski, D., Thöne, C. C., Ramirez-Ruiz, E., et al. 2010, MNRAS, 404, 963
Krimm, H., Barbier, L., Barthelmy, S., et al. 2005, GCN, 3667, 1
Krimm, H., Barbier, L., Barthelmy, S., et al. 2006, GCN, 5704, 1
Krimm, H., Barbier, L., Barthelmy, S. D., et al. 2007, GCN, 6732, 1
Krimm, H. A., Barthelmy, S. D., Baumgartner, W. H., et al. 2009, GCN, 9551, 1
Kruckow, M. U., Tauris, T. M., Langer, N., Kramer, M., & Izzard, R. G. 2018, MNRAS, 481, 1908
Krühler, T., Malesani, D., Fynbo, J. P. U., et al. 2015, A&A, 581, A125
Küpcü Yoldaş, A., Krühler, T., Greiner, J., et al. 2008, in AIP Conf. Proc. 1000, Gamma-Ray Bursts 2007, ed. M. Galassi, D. Palmer, & E. Fenimore (Melville, NY: AIP), 227
Kuroda, D., Yanagisawa, K., Shimizu, Y., et al. 2010, GCN, 11487, 1
Landsman, W., & Krimm, H. A. 2010, GCN, 11490, 1
Lattimer, J. M., & Schramm, D. N. 1974, ApJL, 192, L145
Leibler, C. N., & Berger, E. 2010, ApJ, 725, 1202
Levan, A. J., Curran, P., Wiersema, K., & Groot, P. 2009, GCN, 9547, 1
Levan, A. J., & Tanvir, N. R. 2013, GCN, 14667, 1
Li, L.-X., & Paczynski, B. 1998, ApJL, 507, L59
Lyman, J. D., Levan, A. J., Tanvir, N. R., et al. 2017, MNRAS, 467, 1795
Mahajan, S., Ashby, M. L. N., Willner, S. P., et al. 2019, MNRAS, 482, 560
Malesani, D., Covino, S., D'Avanzo, P., et al. 2007, A&A, 473, 77
Malesani, D., Stella, L., Covino, S., et al. 2006a, GCN, 5705, 1
Malesani, D., Stella, L., D'Avanzo, P., et al. 2006b, GCN, 5718, 1
Mannucci, F., Cresci, G., Maiolino, R., et al. 2009, MNRAS, 398, 1915
Mapelli, M., Giacobbo, N., Toffano, M., et al. 2018, MNRAS, 481, 5324
Margalit, B., & Piran, T. 2015, MNRAS, 452, 3419
Markwardt, C., Barbier, L., Barthelmy, S. D., et al. 2006, GCN, 5882, 1
Markwardt, C. B., Barthelmy, S. D., Baumgartner, W. H., et al. 2010a, GCN, 11111, 1
Markwardt, C. B., Barthelmy, S. D., Baumgartner, W. H., et al. 2010b, GCN, 11486, 1
McMullin, J. P., Waters, B., Schiebel, D., Young, W., & Golap, K. 2007, in ASP Conf. Ser. 376, Astronomical Data Analysis Software and Systems XVI, ed. R. A. Shaw, F. Hill, & D. J. Bell (San Francisco, CA: ASP), 127
Metzger, B. D., & Bower, G. C. 2014, MNRAS, 437, 1821
Michałowski, M., Hjorth, J., & Watson, D. 2010, A&A, 514, A67
Michałowski, M. J., Kamble, A., Hjorth, J., et al. 2012, ApJ, 755, 85
Murphy, E. J., Condon, J. J., Schinnerer, E., et al. 2011, ApJ, 737, 67
Nakar, E., & Piran, T. 2011, Natur, 478, 82
Nicuesa Guelbenzu, A., Klose, S., Greiner, J., et al. 2012, A&A, 548, A101
Nicuesa Guelbenzu, A., Klose, S., Michałowski, M. J., et al. 2014, ApJ, 789, 45

Nicuesa Guelbenzu, A., Klose, S., Palazzi, E., et al. 2015, A&A, 583, A88
Norris, J., Ukwatta, T. N., Barthelmy, S. D., et al. 2010, GCN, 11113, 1
Nugent, P. E., & Bloom, J. S. 2010, GCN, 11491, 1
Nysewander, M., Fruchter, A. S., & Pe'er, A. 2009, ApJ, 701, 824
Oates, S. R., Barthelmy, S. D., Beardmore, A. P., et al. 2010, GCN, 11102, 1
Pagani, C., & Krimm, H. A. 2010, GCN, 11488, 1
Palmer, D., Barbier, L., Barthelmy, S. D., et al. 2006, GCN, 5905, 1
Parsons, A., Barbier, L., Barthelmy, S. D., et al. 2007, GCN, 6656, 1
Pérez-Ramírez, D., Norris, J. P., Gorosabel, J., et al. 2013, in Gamma-ray Bursts: 15 Years of GRB Afterglows, ed. A. J. Castro-Tirado, J. Gorosabel, & I. H. Park (Les Ulis: EDP), 345
Perley, D. A., Bloom, J. S., Modjaz, M., et al. 2008, GCN, 7889, 1
Perley, D. A., Hjorth, J., Tanvir, N. R., & Perley, R. A. 2017, MNRAS, 465, 970
Perley, D. A., Modjaz, M., Morgan, A. N., et al. 2012, ApJ, 758, 122
Perley, D. A., & Perley, R. A. 2013, ApJ, 778, 172
Perley, D. A., Perley, R. A., Hjorth, J., et al. 2015, ApJ, 801, 102
Peters, C., van der Horst, A. J., Chomiuk, L., et al. 2019, ApJ, 872, 28
Planck Collaboration, Ade, P. A. R., Aghanim, N., et al. 2016, A&A, 594, A13
Prochaska, J. X., Bloom, J. S., Chen, H.-W., et al. 2006, ApJ, 642, 989
Radice, D., Perego, A., Hotokezaka, K., et al. 2018, ApJ, 869, 130
Resmi, L., & Zhang, B. 2016, ApJ, 825, 48
Rossi, A., Stratta, G., Maiorano, E., et al. 2019, arXiv:1901.05792
Sakamoto, T., Barthelmy, S. D., Baumgartner, W. H., et al. 2010, GCN, 10379, 1
Sato, G., Barbier, L., Barthelmy, S., et al. 2006, GCN, 5064, 1
Sato, G., Barbier, L., Barthelmy, S. D., et al. 2007, GCN, 6681, 1
Sault, R. J., Teuben, P. J., & Wright, M. C. H. 1995, in ASP Conf. Ser. 77, Astronomical Data Analysis Software and Systems IV, ed. R. A. Shaw, H. E. Payne, & J. J. E. Hayes (San Francisco, CA: ASP), 433
Savaglio, S., Glazebrook, K., & Le Borgne, D. 2009, ApJ, 691, 182
Schlegel, D. J., Finkbeiner, D. P., & Davis, M. 1998, ApJ, 500, 525
Silva, L., Granato, G. L., Bressan, A., & Danese, L. 1998, ApJ, 509, 103
Smartt, S. J., Chen, T.-W., Jerkstrand, A., et al. 2017, Natur, 551, 75
Sokolov, V. V., Fatkhullin, T. A., Castro-Tirado, A. J., et al. 2001, A&A, 372, 438
Stanway, E. R., Davies, L. J. M., & Levan, A. J. 2010, MNRAS, 409, L74
Stanway, E. R., Levan, A. J., & Davies, L. J. M. 2014, MNRAS, 444, 2133
Stratta, G., D'Avanzo, P., Piranomonte, S., et al. 2007, A&A, 474, 827
Symbalisty, E., & Schramm, D. N. 1982, ApJL, 22, L143
Tabatabaei, F. S., Schinnerer, E., Krause, M., et al. 2017, ApJ, 836, 185
Tanvir, N. R., Levan, A. J., Fruchter, A. S., et al. 2013, Natur, 500, 547
Tanvir, N. R., Levan, A. J., Fruchter, A. S., et al. 2015, GCN, 18100, 1
Tanvir, N. R., Vergani, S., Hjorth, J., et al. 2010, GCN, 11123, 1
Tauris, T. M., Kramer, M., Freire, P. C. C., et al. 2017, ApJ, 846, 170
Tisanić, K., Smolčić, V., Delhaize, J., et al. 2019, A&A, 621, A139
Tueller, J., Barthelmy, S. D., Cummings, J., et al. 2008, GCN, 7205, 1
Tunnicliffe, R. L., & Levan, A. 2012, in IAU Symp. 279, Death of Massive Stars: Supernovae and Gamma-Ray Bursts, ed. P. Roming, N. Kawai, & E. Pian (Cambridge: Cambridge Univ. Press), 415
Uehara, T., Ohno, M., Takahashi, T., et al. 2008, GCN, 7223, 1
Urata, Y., Tashiro, M., Abe, K., et al. 2006a, GCN, 5717, 1
Urata, Y., Tashiro, M., Abe, K., et al. 2006b, GCN, 5917, 1
van der Horst, A. J., Kamble, A., Resmi, L., et al. 2008, A&A, 480, 35
von Kienlin, A. 2010, GCN, 10381, 1
Voss, R., & Tauris, T. M. 2003, MNRAS, 342, 1169
Wainwright, C., Berger, E., & Penprase, B. E. 2007, ApJ, 657, 367
Wanderman, D., & Piran, T. 2015, MNRAS, 448, 3026
Wilson, W. E., Ferris, R. H., Axtens, P., et al. 2011, MNRAS, 416, 832
Woosley, S. E., & Bloom, J. S. 2006, ARA&A, 44, 507
Wright, E. L., Eisenhardt, P. R. M., Mainzer, A. K., et al. 2010, AJ, 140, 1868
Xie, C., Fang, T., Wang, J., Liu, T., & Jiang, X. 2016, ApJL, 824, L17
Xu, D., Ilyin, I., & Fynbo, J. P. U. 2010, GCN, 11492, 1
Zauderer, A., Berger, E., & Fong, W. 2011, GCN, 11620, 1
Zhang, S., Jin, Z.-P., Wang, Y.-Z., & Wei, D.-M. 2017, ApJ, 835, 73